STRUCTURE-COUPLED MULTIPHYSICS IMAGING IN GEOPHYSICAL SCIENCES

Luis A. Gallardo[1] and Max A. Meju[2,3]

Received 3 March 2010; revised 1 December 2010; accepted 18 January 2011; published 3 March 2011.

[1] Multiphysics imaging or data inversion is of growing importance in many branches of science and engineering. In geophysical sciences, there is a need for combining information from multiple images acquired using different imaging devices and/or modalities because of the potential for accurate predictions. The major challenges are how to combine disparate data from unrelated physical phenomena, taking into account the different spatial scales of the measurement devices, model complexities, and how to quantify the associated uncertainties. This review paper summarizes the role played by the structural gradients-based approach for coupling fundamentally different physical fields in (mainly) geophysical inversion, develops further understanding of this approach to guide newcomers to the field, and defines the main challenges and directions for future research that may be useful in other fields of science and engineering.

Citation: Gallardo, L. A., and M. A. Meju (2011), Structure-coupled multiphysics imaging in geophysical sciences, *Rev. Geophys.*, *49*, RG1003, doi:10.1029/2010RG000330.

1. INTRODUCTION

[2] Direct and indirect measurements of different properties of physical systems such as the Earth and human body are often made at different spatial and temporal scales. Such multidimensional, multispectral and often incomplete heterogeneous data sets are used to infer the structure and physical state of the system under investigation. In many cases, detecting and monitoring the presence or movement of fluids within such systems from multimodal signal sensing and imaging are a primary objective for several reasons, and require accurate knowledge of the structure holding or confining the fluids. In the Earth sciences for instance, accurate characterization of material heterogeneity and its influence on fluid flow or storage in subterranean reservoirs is of crucial importance in a wide range of contemporary issues including the use of groundwater resources, volcano and earthquake monitoring, methane storage in wetlands, carbon dioxide sequestration and efficient extraction of fossil fuels and landfill methane [e.g., *Beckwith and Baird*, 2001; *Hertrich and Yaramanci*, 2002; *Binley et al.*, 2002; *Gedney et al.*, 2004; *Roecker et al.*, 2004; *Comas et al.*, 2005; *Chen et al.*, 2006; *Alpak et al.*, 2004, 2008; *Bedrosian et al.*, 2007]. (A glossary of some common geophysical terms is included and their first appearance is in italics). Interactions between fluid and solid mineral components of subterranean reservoirs can generate or allow the transmission of electrochemical, *electromagnetic* and mechanical signals that can be measured using geophysical methods and inverted to image the subsurface physical property distribution [e.g., *Berge et al.*, 2000; *Hubbard et al.*, 2006]. However, while imaging methods based on *electrical* [*Sasaki*, 2004; *Günther et al.*, 2006], electromagnetic [e.g., *Rodi and Mackie*, 2001; *Sasaki and Meju*, 2006a, 2006b; *Commer and Newman*, 2008], *nuclear magnetic resonance* [*Hertrich and Yaramanci*, 2002] and sound wave or *seismic* [*Bergman et al.*, 2004; *Hole et al.*, 2005] phenomena are well established in geophysical studies of fluid reservoirs, there are still limitations in the way that the data from multidimensional imaging surveys are interpreted, and a unique noninvasive definition of reservoir structure and presence of fluids has so far remained a difficult and uncertain proposition.

[3] In medical imaging among others, combining information from multiple images acquired using different patient scanning devices and/or modalities and at different times, the so-called image fusion, is a major challenge [*Haber and Modersitzki*, 2007; *Dullin et al.*, 2009 and references therein]. Multimodal image registration combines the strengths of different imaging modalities by aligning images from different sources for fusion, but there are still difficulties in medical image processing as enumerated elsewhere [*Haber and Modersitzki*, 2007; *Handels et al.*, 2007].

[4] The major difficulty has been how to combine the disparate data from unrelated physical or physiochemical phenomena and taking into account the different spatial

[1]School of Earth and Environment, University of Western Australia, Crawley, Western Australia, Australia.
[2]Lancaster Environmental Centre, Lancaster University, Lancaster, UK.
[3]Now at Petronas Research, Kajang, Malaysia.

8755-1209/11/2010RG000330
Paper number 2010RG000330

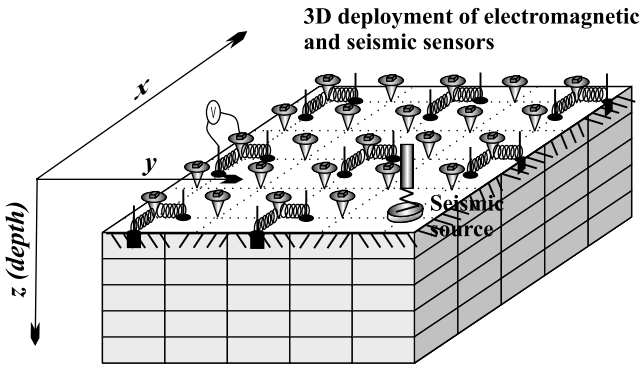

Figure 1. Illustration of the concept of multiphysics or multimodal remote sensing measurements. An array of sources and detectors are deployed within, above, or on the surface of a physical system. The detectors or sensors register data related to the object's response to physical excitations of the system by the different applied sources.

scales (or footprints) of the numerous available methods of remote sensing, scanning or depth sounding (see, e.g., Figure 1). This challenge is compounded further by the lack of established procedures for characterization and propagation of uncertainties in the measured data and model predictions, and our often limited or incomplete knowledge of the physical system being imaged. The measured data are typically of limited bandwidth and may be corrupted by ambient noise, and are at best described as inaccurate, insufficient and inconsistent [*Jackson*, 1972] for a unique characterization of the physical system. The natural physical systems are complex and our physics-based models describing them are only as good as the limited information available about the natural world. Thus, in essence, there is unavoidable discrepancy between physics-based predictions of the system response and the realities they purport to represent. So, how can we overcome these difficulties and generate more realistic images of a physical system? Multiphysics-based imaging and uncertainty analysis have the potential to provide an answer to this question as is long known in geophysical imaging [*Vozoff and Jupp*, 1975] but the emphasis in multidimensional analysis has been on modeling measurements from physically related phenomena, for which there are empirically observed or analytically established relationships [e.g., *Lines et al.*, 1988; *Sasaki*, 1989; *Lees and VanDecar*, 1991; *Oldenburg et al.*, 1997; *Paasche and Tronicke*, 2007]. Combining data sets from uncorrelated physical processes is more challenging and this has prompted vigorous research in process coupling, uncertainty quantification, and interpretation of resultant models in terms of the attendant physical processes.

[5] The purpose of this review is to summarize the role played by the structural gradients-based approach for coupling fundamentally different physical fields in (mainly) geophysical inversion (section 2), develop further understanding of this approach to guide newcomers to the field of multiphysics inversion (sections 3 and 4), and define the main challenges for future research (section 5). Although we draw mostly from the geophysical literature, we develop the necessary background material in tutorial form in section 3 and provide a glossary of geophysical terms to make this paper accessible to workers in different fields in which physics-based process simulation (forward modeling) apply. In section 3, we explore some metrics for quantification of uncertainty in gradient-based image reconstruction or integration of multiphysics information. Given the large-scale needs of the geosciences community, we also draw attention to variance-covariance estimation by Monte Carlo integration as an attractive approach to uncertainty quantification [e.g., *Alkhatib and Schuh*, 2007]. In section 4, we demonstrate an emerging joint inversion approach that combines multiphysics and geological information derived principally from boreholes so as to improve images of subsurface structures [*Gallardo*, 2007b; *Cardiff and Kitanidis*, 2009; *Lelièvre and Oldenburg*, 2009]. This approach is significant because the ultimate challenge of incorporating borehole constraints in appropriately coupled three-dimensional (3-D) imaging of spatial and temporal field measurements which respond to electrical, chemical and mechanical excitations of a physical system such as the Earth will permit a realistic characterization of its structural heterogeneity and the possible influence on fluid transport. Interestingly, the physics of fluid flow and electromagnetic induction or sound propagation phenomena in porous media can be coupled through fluid saturation equations [*Pride*, 1994; *Alpak et al.*, 2008]. Consequently, we explore new directions in the use of a fluid transport model to link geophysical inversion results to the microscopic properties of rocks which control subterranean fluid flow [*Cassiani and Binley*, 2005; *Linde et al.*, 2006; *Alpak et al.*, 2008; *Looms et al.*, 2008], and discuss the outstanding challenges and suggest directions for future research in multiphysics imaging in section 5.

2. WHAT IS STRUCTURE-COUPLED JOINT INVERSION?

2.1. Structural Coupling of Multiphysics Inverse Problems

[6] Apart from some well-known process couplings such as the effect of temperature and fluid saturation on electromagnetic and sound wave propagation in porous media [*del Río and Whitaker*, 2001; *Pride*, 1994], the couplings between the physical theories used to predict the outcomes of many multiphysics experiments on a natural physical system may be largely uncertain, and their stability and convergence properties unknown. There are thus significant challenges in any combined analysis of these possibly complex nonlinear and time-dependent phenomena. Consequently, experimental data from coincidentally located seismic and electrical or electromagnetic multidimensional scanning of the Earth (Figure 1) are commonly inverted separately since there is no established analytical relationship between these depth-scanning methods. Separate data inversion leads to inconsistent models for the same subsurface target under observation. Moreover, individual physical phenomena such as sensed in geophysical experiments are subject to attenua-

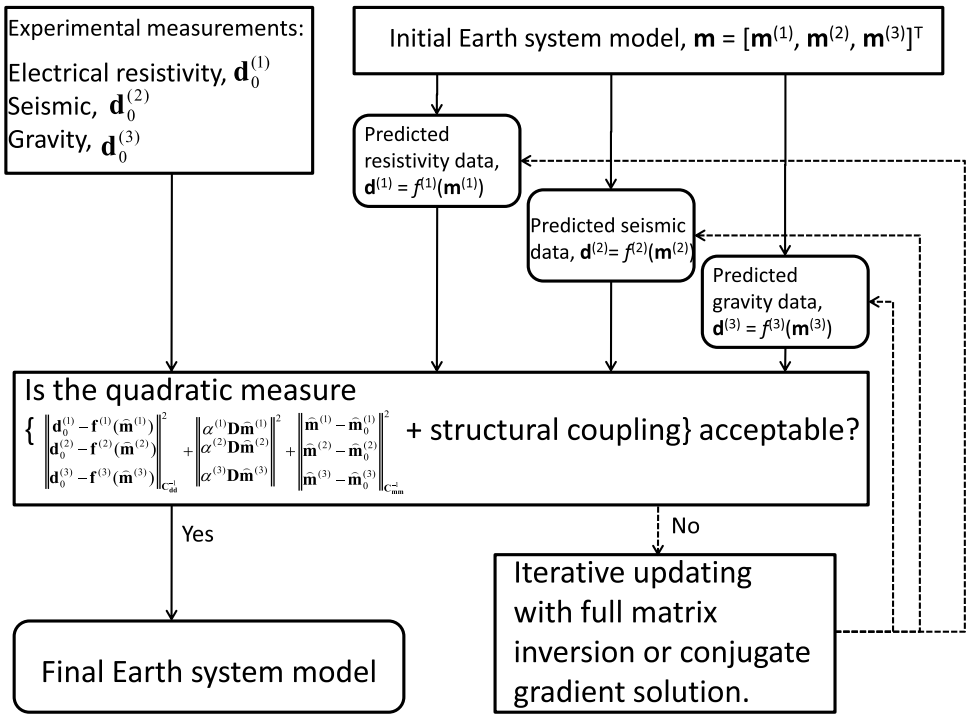

Figure 2. Flowchart of a basic structure-coupled multiphysics imaging of an Earth system using geophysical measurements. A quadratic measure is minimized under the imposed condition of structural similarity, enforced on the unknown models for the different physical property fields (resistivity, velocity, density). The matrix D and the weighting factor α serve for the regularization of the problem while the available prior knowledge of the system parameters is contained in $\mathbf{m}_0$.

tive and dispersive processes which along with our limited knowledge of the physical system, limit the resolution capabilities of the typically band-limited experimental data. However, just as rock porosity and the presence and amount of fluids can influence the electrical and mechanical properties of porous media [*Pride*, 1994], the structural attributes of the media can influence the interactions between these properties and any applied electrical, electromagnetic and mechanical excitations. In geophysical imaging, the rock structure or boundaries may remain common to the multiphysics scanning methods (i.e., a common frame of reference) and thus serve for multiple property coupling and integration, which can help reduce the model uncertainty inherent in using the individual methods. This is the basis of structure-coupled joint inversion. Structural coupling requires the imposition of physically or mathematically driven matching conditions at structural boundaries in a numerically stable way. An appropriate measure of data misfit is minimized subject to the conditions of structural similarity enforced on the sought physical models (Figure 2). Simultaneous multidimensional inverse modeling or "joint inversion" of multiphysics data with structural constraints (Figure 2) has been shown to lead to models that are in better accord and closer to the true system property distribution [*Haber and Oldenburg*, 1997; *Zhang and Morgan*, 1997; *Berge et al.*, 2000; *Ditmar*, 2002; *Musil et al.*, 2003; *Gallardo and Meju*, 2003, 2004, 2007; *Meju*, 2005; *Chen et al.*, 2006; *Linde et al.*, 2006, 2008; *Bedrosian*, 2007; *Bedrosian et al.*, 2007; *Gallardo* 2007a; *Hu et al.*, 2007; *Infante et al.*, 2010]. However, not all physical property distributions in the subsurface will be structurally coincident and some flexibility in model reconstruction may be necessary in some geological environments.

[7] We distinguish between structure-coupled joint inversion of multiphysics data [e.g., *Gallardo and Meju*, 2003] and the alternative approach of traditional cooperative inversion [*Lines et al.*, 1988; *Oldenburg et al.*, 1997; *Paasche and Tronicke*, 2007] or structural cooperative inversion [e.g., *Lelièvre*, 2009; *Jegen et al.*, 2009]. In the iterative cooperative inversion of data from two geophysical methods, the respective data sets are inverted in separated steps but the resulting model (i.e., structure and physical property distribution) of one iteration step is used as the starting model for the other step through an assumed relation between the two methods. Some (compositional) correlation between the physical properties is assumed in the traditional cooperative inversion approach while it is assumed that the structural aspects of the physical property fields are spatially correlated in structural cooperative inversion. This approach may not lead to a unique solution but allows for the possibility that not all geophysical attributes are structurally coupled. It is possible to constrain the cooperative solution process to honor a priori structural information about the physical system but our knowledge of the system is often incomplete and may be inconsistent with the experimental data. There is thus a need for an approach to resolve or avoid such potential conflicts with measured data. It is emerging that appropriately coupled simultaneous inversion of multiphysics data with a priori information (Figure 2) might provide a

panacea for such problems [*Gallardo*, 2007b; *Cardiff and Kitanidis*, 2009; *Lelièvre and Oldenburg*, 2009].

2.2. Quantifying Uncertainty in Multiphysics Joint Inversion

[8] Although coupled multiphysics imaging can lead to realistic models of a physical system, an essential element in decision making with such models is an understanding of the range of possible solutions permitted by the inverted band-limited heterogeneous data. Accurate characterization of model uncertainty is critical for evaluating risk in high-stake operations like oil field prospect evaluation and development where it drives business decisions such as the well placement and well count. From an imaging point of view, the key sources of uncertainty are data inaccuracy and limited bandwidth, incomplete knowledge and information about the typically complex physical system under investigation, and predictive modeling (theoretical and discretization) errors. These sources of uncertainty have been treated using either deterministic or probabilistic approaches [see, e.g., *DeVolder et al.*, 2002; *Reagan et al.*, 2003; *Caers et al.*, 2006; *Chappell and Lancaster*, 2007; *Vasco*, 2007; *Cardiff and Kitanidis*, 2009; *Meju*, 2009 and references therein]. A particularly difficult challenge is error estimation in the solution of partial differential equations that constitute our numerical representation of the physical system being investigated [e.g., *DeVolder et al.*, 2002; *Reagan et al.*, 2003]. In the presence of limited information about a complex physical system, uncertainty may arise in the selection of the relevant physics and associated models, approximations in the experiments used for validating these process simulation models, and the computationally achievable model resolutions with the available machines. However, its quantification has emerged over the past decade as a body of knowledge that can permit meaningful model-based predictions of physicochemical phenomena [e.g., *Reagan et al.*, 2003]. Unfortunately, metrics for validating predictions of physical reality and mathematical constructs that are useful for describing uncertainties in multidimensional multiphysics imaging are lacking, making practical interpretation of model predictability and uncertainty in data inversion a difficult proposition. Many approaches have been proposed to quantify this uncertainty in multidimensional inverse modeling. The deterministic approaches include linear sensitivity analysis [e.g., *Alumbaugh and Newman*, 2000; *Kalscheuer and Pedersen*, 2007; *Kalscheuer et al.*, 2010] and construction of extremal solutions [e.g., *Vasco*, 2007; *Meju*, 2009]. The probabilistic approaches include density function estimation [*Snieder*, 2004; *Caers et al.*, 2006; *Cardiff and Kitanidis*, 2009] and covariance estimation by Monte Carlo integration [e.g., *Alkhatib and Schuh*, 2007]. The key question here is, can we realistically quantify uncertainty in large-scale applications of structure-coupled multiphysics imaging?

2.3. Post Inversion Classification and Interpretation of System Parameters

[9] In spite of the recent developments in structure-coupled joint inversion, the idea of unique determination of structural and compositional trends of a physical system such as the Earth's crust from joint inverse modeling still faces conceptual and technical challenges. As result, the classification of structure and *lithology* (or *lithofacies*) based on multiphysics imaging has received the attention of several workers [*Bosch*, 1999; *Bosch et al.*, 2002; *Gallardo and Meju*, 2003, 2007; *Günther and Bentley*, 2006; *Paasche et al.*, 2006; *Bedrosian et al.*, 2007; *Paasche and Tronicke*, 2007; *Linde et al.*, 2008; *Infante et al.*, 2010]. *Gallardo and Meju* [2003] introduced a simple concept of using the result of joint inversion for structural and lithological classification. For an imaging problem involving two or more physical fields such as electrical resistivity and sound wave velocity, they perform pixel-by-pixel search for correlated patterns in the jointly reconstructed images. The various trends were then used to infer geological associations such as distinct lithological units within each common structural entity in the reconstructed model of the subsurface. This concept was investigated by other workers with variable conclusions [*Linde et al.*, 2006, 2008; *Günther and Bentley*, 2006; *Paasche et al.*, 2006; *Bedrosian et al.*, 2007; *Gallardo and Meju*, 2007; *Paasche and Tronicke*, 2007; *Infante et al.*, 2010]. The issue of contention is how the zones of similar physical property trends are selected and classified. Some workers suggest that the identified patterns may be an artifact of the regularization used in solving the joint inverse problem and/or bias on the part of the interpreter [*Bedrosian et al.*, 2007]. *Günther and Bentley* [2006] employed cluster analysis for trend selection in their structure-coupled joint electrical resistivity and seismic velocity models. *Gallardo and Meju* [2007] investigated the effect of different problem regularizations on 2-D structure-coupled joint inversion of synthetic and field data. They showed that there are well defined trends in the reconstructed models which may permit structural and lithological classification.

[10] *Linde et al.* [2006] constructed 3-D joint inversion models from *cross-hole* electrical resistivity and *georadar* travel time measurements and used the results, validated against borehole data, to investigate the lithological classification problem. Joint inversion made it possible for them to estimate probability density functions of subsurface formation factor, the water content, and the effective grain radius of the sediments in the different zones identified using the classification concept of *Gallardo and Meju* [2003]. Their estimates were consistent with *gamma ray* logs, measured clay fractions, and electrical *formation factors* in a cored borehole. Is realistic structural and lithological classification possible without sufficient knowledge and information about physical reality? *Linde et al.* [2008] applied a structure-coupled joint inversion method to a well-instrumented control site where the geology consists of saturated unconsolidated sediments with 3-D heterogeneity. They found that the highest correlation between inferences from joint inversion and comparative flowmeter measurements in boreholes were obtained when a priori information (in the form of a stochastic regularization operator) was incorporated in the problem formulation. *Infante et al.* [2010] conducted coincidentally located electrical resistivity and seismic travel time mea-

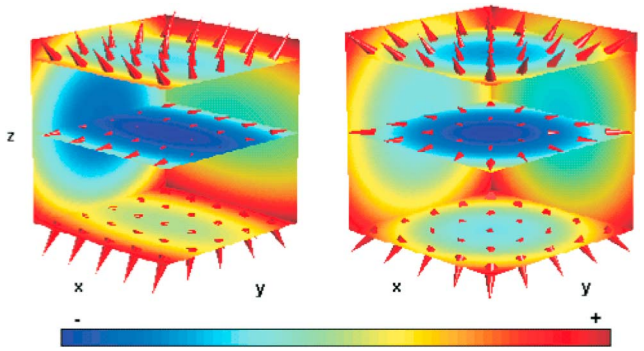

Figure 3. Gradient fields of two geometrical volumes (ellipsoidal and spherical shells). Note that differences in the shapes are observed in the direction of the gradient vectors, whereas the gradient magnitudes are arbitrarily set as constant [after *Fregoso*, 2010].

surements along two profiles at a controlled site where geotechnical data were available from boreholes for validation. The available data on sediment types, thicknesses and moisture content were determined independently using standard geotechnical methods. The result of 2-D structure-coupled joint inversion for resistivity and seismic velocity correlated remarkably well with the geotechnical information along both measurement profiles, thus establishing that structural and lithological (including water content) classification is possible with well-implemented joint inversion. However, the accuracy of any joint inversion approach can be improved by incorporating reliable extraneous information about the physical system being investigated. The key question here is, how can we fully integrate hard and soft information about physical reality in joint inversion? In what follows, we will suggest how the questions highlighted above may be addressed. First, we provide a tutorial that serves as the starting point for newcomers to the field of structural joint inversion.

3. SOLUTION OF MULTIPHYSICS INVERSE PROBLEMS BASED ON COMMON STRUCTURE

3.1. Preliminaries: Gradient-Based Measures of Image Similarity

3.1.1. Direction-Dependent Measures

[11] The similarities or differences in the gradients direction of any two images can be measured using a variety of multidimensional operators. A simple comparison of properly normalized directions is given by measures such as the normalized gauss map function [*Droske and Rumpf*, 2004]

$$\hat{n} = \frac{\nabla m}{\|\nabla m\|}, \tag{1}$$

where ∇m is the gradient of an image. This function (1) describes the precise direction vector of the physical property fields (see Figure 3) but for normalized gradients, singularities can occur when $\|\nabla m\| \rightarrow 0$ such as in homogenous media, local maxima-minima and saddle points.

[12] The simple difference between two appropriately normalized image gradients

$$\Delta\vec{\phi} = \hat{n}^{(1)} - \hat{n}^{(2)}, \tag{2}$$

provides a linear comparison of the structural resemblance of two images and has significant computational advantages. *Droske and Rumpf* [2004] show successful applications of this approach to medical image registration where careful attention was given to the singularity arising from (1) by a supervised selection of remarkable features with large property gradients for the application of (2).

[13] Another approach employs either angular or trigonometric functions as gradient measures. *Droske and Rumpf* [2004] discuss product-related functions based on normalized gauss maps and propose functions such as

$$\Delta\phi = \hat{n}^{(1)} \bullet \hat{n}^{(2)} \tag{3}$$

and

$$\Delta\vec{\phi} = \hat{\mathbf{n}}^{(1)} - \hat{\mathbf{n}}^{(2)}\left(\hat{\mathbf{n}}^{(1)} \bullet \hat{\mathbf{n}}^{(2)}\right). \tag{4}$$

The biggest drawback of these functions is the combination of the singularities associated with both normalized image gradients. Similarly, *Gallardo and Meju* [2004] propose the use of angles and vector products based on gradients and suggest functions such as

$$\theta(x,y,z) = \cos^{-1}\left(\hat{n}^{(1)} \bullet \hat{n}^{(2)}\right) \tag{5}$$

and

$$\Delta\phi = \frac{1}{1 - \hat{n}^{(1)} \bullet \hat{n}^{(2)}}. \tag{6}$$

However, these not only face the problem of combined singularities of two gauss map functions but also the additional nonlinearity of the trigonometric functions and their periodicity-related discontinuity.

[14] Alternative unnormalized functions based on vector products have been proposed. Remarkably, the cross-gradient function [*Gallardo and Meju*, 2003] defined as

$$\vec{\tau} = \nabla m^{(1)} \times \nabla m^{(2)}, \tag{7}$$

has proven useful and stable, and its application has steadily grown in joint multiphysics inverse problems [*Fregoso and Gallardo*, 2009; *Gallardo and Meju*, 2003, 2004; *Gallardo et al.*, 2005; *Gallardo*, 2007a; *Gallardo and Meju*, 2007; *Hu et al.*, 2009; *Infante et al.*, 2010; *Linde et al.*, 2006, 2008; *Tryggvason and Linde*, 2006]. The multiplicative character of this function does not demand additional normalizations/equalizations or angular transformations. It shows no discontinuities or singularities and can detect differences within large or small gradients. Figure 4 shows a three-dimensional map of this function for two 3-D objects (ellipsoidal and spherical shells) with rotation geometry [*Fregoso and Gallardo*, 2009]. The direction of the cross-gradient vector is consistent with the circular geometry of the objects whereas the

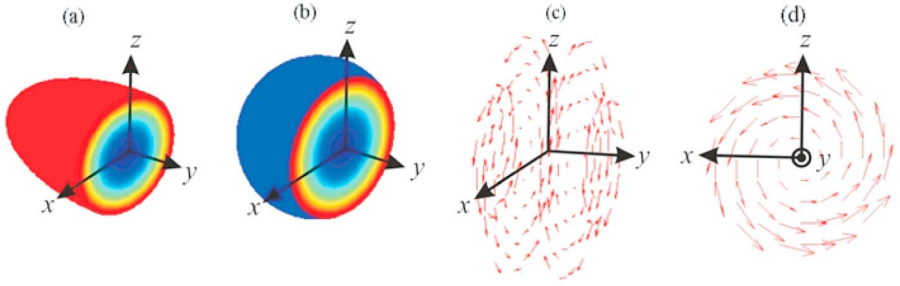

Figure 4. Comparison of (a) ellipsoidal and (b) spherical images to determine their 3-D structural resemblance. (c) A perspective view of four selected vertical slices that show the cross-gradient vectors for these models. Note the (d) circular *y*-*z* behavior of the cross-gradients and the partial 2-D resemblance indicated by the null x component of all cross-gradient vectors [after *Fregoso and Gallardo*, 2009].

magnitude of the vector emphasizes the morphological differences due to conflicting gradients. Note that common structures are picked up when the magnitudes of the three components of the cross-gradient vector are zero. Also, the specific components of the cross-gradient vectors that are equal to zero show the structural similarity in a consistent geometrical direction. For instance, the radial geometry in Figure 4 reduces two components (radial and x direction) of the cross-gradient vector to zero, whereas a two-dimensional geometry reduces the vector to just its transverse component [see *Gallardo et al.*, 2005, Figure 1]. In the general three-dimensional (3-D) objects, if a coordinate basis can align parallel to the equivalent (equipotential) geometrical contours, it will reduce the need for the whole cross-gradient vector to that of just one component, which is computationally advantageous. Unfortunately, the determination of this particular axis in images of multidimensional objects is a complex task.

3.1.2. Direction-Independent Measures

[15] A different approach to measuring structural resemblance uses the magnitude of the gradient fields and ignores the directional characteristic of the property changes [e.g., *Cumani*, 1991; *Toivanen et al.*, 2003]. When this strategy is applied to pattern recognition tasks such as edge detection, the gradients that are regarded as large are simply selected as the most appropriate to define the edges of the objects. This is measured by a threshold value which can be statistically regulated so as to guarantee that the amplitude of the change surpasses the noise level in the image. For geophysical imaging involving two different data sets, *Haber and Oldenburg* [1997] and *Zhang and Morgan* [1997] propose the use of model curvature as a measure of structure. *Haber and Oldenburg* [1997] employ the function

$$\phi = \begin{cases} 0 & |\nabla^2 m| < \tau_1 \\ P_5(|\nabla^2 m|) & \tau_1 < |\nabla^2 m| < \tau_2 \\ 1 & \tau_2 < |\nabla^2 m|, \end{cases} \tag{8}$$

while *Zhang and Morgan* [1997] use a function of the form

$$\phi = \frac{\|\nabla^2 m\|}{\alpha^2}, \tag{9}$$

as a structure operator. In equations (8) and (9), P_5 is a one-dimensional polynomial of degree 5 which makes the structure operator twice Frechet differentiable, τ_1 and τ_2 define the interval within which this operator is twice differentiable, and α is an amplitude normalization factor. These functions principally detect the edges of objects in images and the structural differences between the two images is given by

$$\Delta\phi = \phi^{(1)} - \phi^{(2)}. \tag{10}$$

A key feature of this approach is that it assumes that the coincident occurrence of sharp edges or prescribed smoothed edges is the main indicator of morphological resemblance and penalizes other variations such as ramp- or fuzzy-type boundaries. The presumed advantage is that $\Delta\phi$ is a linear operator and this facilitates its computation. However, it requires a model-dependent normalization (which actually suggests its nonlinear nature) and ignores direction-dependent morphological information that defines an object's shape.

3.2. Joint Inversion Based on Gradient Direction of Resemblance

[16] There are two different philosophies on structure-coupled joint inversion. One school of thought seeks exact structural resemblance between the sought images. In the other school of thought, structural resemblance is encouraged, rather than imposed, by minimizing a weighted norm of the structural resemblance constraint. The advantages and drawbacks of each approach are discussed below.

3.2.1. Inversion for Exact Structural Resemblance

[17] *Gallardo and Meju* [2003] use the cross-gradient function (7) in multiphysics imaging and consider two geophysical images, electrical resistivity ($\mathbf{m}^{(1)}$) and seismic velocity ($\mathbf{m}^{(2)}$), of the same object to be structurally similar when

$$\Delta\vec{\phi}_{\mathbf{i}} = \vec{r}_{\mathbf{i}} = \nabla\mathbf{m}^{(1)}(\mathbf{x_i}, \mathbf{y_i}, \mathbf{z_i}) \times \nabla\mathbf{m}^{(2)}(\mathbf{x_i}, \mathbf{y_i}, \mathbf{z_i}) = \vec{0}. \tag{11}$$

The inverse problem is posed as the search for those structurally similar images, as gauged by equation (11),

which satisfy the measured electrical resistivity and seismic travel time data. The data are assumed to contain random noise whose distribution is Gaussian with zero mean and variance $\boldsymbol{\sigma}^2$. Some knowledge of the data covariance matrix $\mathbf{C}_{dd}$ is assumed in terms of the data variances, i.e., $\mathbf{C}_{dd} = \boldsymbol{\sigma}^2\mathbf{I}$. They regularize the problem using smoothness assumptions, and also require the images to honor any available a priori information ($\mathbf{m_0}$) about the sought objects. The errors in the a priori parameter estimates $\mathbf{m}_0$ are assumed to have a Gaussian distribution with covariance matrix $\mathbf{C}_{\mathbf{m}_0\mathbf{m}_0}$ and they minimize the objective function

$$\mathbf{s}(\widehat{\mathbf{m}}^{(1)}, \widehat{\mathbf{m}}^{(2)}) = \left\| \begin{array}{c} \mathbf{d}_0^{(1)} - \mathbf{f}^{(1)}(\widehat{\mathbf{m}}^{(1)}) \\ \mathbf{d}_0^{(2)} - \mathbf{f}^{(2)}(\widehat{\mathbf{m}}^{(2)}) \end{array} \right\|^2_{\mathbf{C}_{\mathbf{dd}}^{-1}} + \left\| \begin{array}{c} \alpha^{(1)}\mathbf{D}\,\widehat{\mathbf{m}}^{(1)} \\ \alpha^{(2)}\mathbf{D}\,\widehat{\mathbf{m}}^{(2)} \end{array} \right\|^2 + \left\| \begin{array}{c} \widehat{\mathbf{m}}^{(1)} - \mathbf{m}_0^{(1)} \\ \widehat{\mathbf{m}}^{(2)} - \mathbf{m}_0^{(2)} \end{array} \right\|^2_{\mathbf{C}^{-1}_{\mathbf{m}_0\mathbf{m}_0}}, \tag{12}$$

subject to $\{\vec{\tau}_i\} = \{\vec{0}\}$ in the discretized model volume. In this expression D is a discrete version of a second-order Tikhonov regularization matrix and is weighted by a constant damping parameter $\alpha^{(\iota)}$ for each model. Note that this essentially biased estimation approach is closely related to the concept of Bayesian inversion [see *Meju*, 1994, 2009]. Since $\mathbf{f}^{(1)}$, $\mathbf{f}^{(2)}$ and $\vec{\tau}$ are nonlinear functions, the solution to the objective function (12) is accomplished by linearizing about a starting model and the minimization proceeds iteratively. The solution at iteration $k + 1$ can be expressed as [*Gallardo and Meju*, 2003]

$$\hat{\mathbf{m}}^{(\mathbf{j})}_{\mathbf{k+1}} = \hat{\mathbf{m}}^{(\mathbf{j})}_{\mathbf{k}} + \mathbf{N}^{(\mathbf{j})^{-1}}_{\mathbf{k}}\left(\mathbf{n}^{(\mathbf{j})}_{\mathbf{k}} - \mathbf{B}^{(\mathbf{j})^{\mathbf{T}}}_{\mathbf{k}}\mathbf{q}_{\mathbf{k}}\right) \quad j = 1, 2. \tag{13}$$

Where

$$\mathbf{N}^{(\mathbf{j})}_{\mathbf{k}} = \mathbf{A}^{(\mathbf{j})^{\mathbf{T}}}_{\mathbf{k}}\mathbf{C}^{(\mathbf{j})^{-1}}_{\mathbf{dd}}\mathbf{A}^{(\mathbf{j})}_{\mathbf{k}} + \alpha^{(\mathbf{j})}\mathbf{D}^{\mathbf{T}}\mathbf{D} + \left(\mathbf{C}^{(\mathbf{j})}_{\mathbf{m}_0\mathbf{m}_0}\right)^{-1}, \tag{14}$$

$$\mathbf{n}^{(j)}_k = \mathbf{A}^{(j)^T}_k\mathbf{C}^{(j)^{-1}}_{dd}\left(\mathbf{d}^{(j)}_0 - \mathbf{f}^{(j)}\left(\hat{\mathbf{m}}^{(j)}_k\right)\right) - \alpha^{(j)}\mathbf{D}^T\mathbf{D}\hat{\mathbf{m}}^{(j)}_k + \left(\mathbf{C}^{(j)}_{m_0m_0}\right)^{-1}\left(\mathbf{m}^{(j)}_0 - \hat{\mathbf{m}}^{(j)}_k\right), \tag{15}$$

$$\mathbf{q}_k = \left\{\mathbf{B}^{(1)}_k\mathbf{N}^{(1)^{-1}}_k\mathbf{B}^{(1)^T}_k + \mathbf{B}^{(2)}_k\mathbf{N}^{(2)^{-1}}_k\mathbf{B}^{(2)^T}_k\right\}^{-1} \cdot \left\{\mathbf{B}^{(1)}_k\mathbf{N}^{(1)^{-1}}_k\mathbf{n}^{(1)}_k + \mathbf{B}^{(2)}_k\mathbf{N}^{(2)^{-1}}_k\mathbf{n}^{(2)}_k + \Delta\phi(\widehat{\mathbf{m}}^{(1)}_k, \widehat{\mathbf{m}}^{(2)}_k)\right\}, \tag{16}$$

$\mathbf{A}_\mathbf{k} = \frac{\partial\mathbf{f}(\mathbf{m})}{\partial\mathbf{m}_\mathbf{k}}$ are the partial derivatives at the point $\mathbf{m} = \hat{\mathbf{m}}_k$, and $\mathbf{B}_k$ is the Jacobian matrix associated with the cross-gradient function. The structural dissimilarity $\Delta\phi$ in equation (16) is measured by the cross-gradient function

$$\tau\left(m^{(1)}, m^{(2)}\right) = \nabla m^{(1)} \times \nabla m^{(2)}, \tag{17}$$

and the partial derivatives of the cross-gradient function are given by a discrete version of the operator

$$\frac{\partial\tau}{\partial m^{(j)}} = \left(\delta_{2,j}\nabla m^{(1)} - \delta_{1,j}\nabla m^{(2)}\right) \times \nabla(\cdot). \tag{18}$$

Using this derivative, a Taylor series expansion about $\widehat{\mathbf{m}}^{(1)}_k$ and $\widehat{\mathbf{m}}^{(2)}_k$ yields

$$\nabla m^{(1)} \times \nabla m^{(2)} \cong \nabla m^{(1)} \times \nabla m^{(2)}_k + \nabla m^{(1)}_k \times \nabla m^{(2)} - \nabla m^{(1)}_k \times \nabla m^{(2)}_k. \tag{19}$$

Therefore,

$$\tau\left(m^{(1)}, m^{(2)}\right) \cong \tau\left(m^{(1)}, m^{(2)}_k\right) + \tau\left(m^{(1)}_k, m^{(2)}\right) - \tau\left(m^{(1)}_k, m^{(2)}_k\right). \tag{20}$$

This equation (20) can be understood as suggesting that in equations (13) to (16), the linearized cross-gradient constraint considers the structural dissimilarities of the previous models $\tau(m^{(1)}_k, m^{(2)}_k)$ when updating both models $\boldsymbol{m}^{(1)}$ and $\boldsymbol{m}^{(2)}$. Following equation (20), it is easy to demonstrate that while the joint inversion algorithm converges, this linearized function will converge toward the exact cross-gradient constraint required to fully enforce the sought structural resemblance.

[18] Note that for 3-D inverse problems, the formulation given by equation (12) leads to an overconstrained problem since it results in three equality constraints on two properties per image cell. In this case, the direct solution of equation (16) leads to numerical inaccuracies and singularity. The constraint Jacobian, $\mathbf{B}_k$, must have full row rank, otherwise the null-space of $\mathbf{B}_k$ or its transpose could be activated leading to numerical instabilities in iterative inversion. An effective strategy for solving this problem in the exact approach involves the removal of redundant constraints from $\mathbf{B}_k$ based on geometrical simplifications (such as two-dimensional formulation) or using the singular value decomposition (SVD) or other factorizations [see *Nocedal and Wright*, 1999]. *Fregoso and Gallardo* [2009] and *Fregoso* [2010] solved this problem in their full 3-D formulation by reducing the row rank of $\mathbf{B}_k$ using the SVD method.

[19] Can any number of physical property fields be combined using this exact resemblance approach and what are its limitations? For the general case of multiple image representations where we have at least k-types of experimental measurements of k different properties of the same object, *Gallardo* [2007a] generalized the method to handle k property fields. In the illustrative two-dimensional joint inversion of four different property fields, each method benefited structurally from the contribution from the other methods [see *Gallardo*, 2007a, Figure 3]. Note that there are some drawbacks in the exact structural approach. The algorithm relies on the measure of structural resemblance for an accurate reconstruction of the shape of the sought object. There is also the possibility of solution equivalency since the information provided by the resemblance measure

can lead to multiple suitable structural models. However, a good algorithm for enforcing similar structure should be able to find the most acceptable solution from among all the structurally equivalent data consistent images of the sought object.

3.2.2. Inversion With Inexact Structural Resemblance Measures

[20] A second school of thought adopts inexact measures of structural resemblance but have the added flexibility that such measures may be treated as statistical realizations, and the solution of the inverse problem can be tailored to meet specific requirements for large-scale systems. *Tryggvason and Linde* [2006], *Linde et al.* [2006, 2008], and *Hu et al.* [2009] adopt this philosophy and form objective functions that include the cross-gradient constraint. It is instructive to show the connection to the exact approach before exploring the various approaches adopted by these workers. If the structural resemblance measure in equation (12) is assumed to be inaccurate and hence assigned an a priori value ($\Delta\phi_o$) with associated covariance matrix $\mathbf{C}_{\phi\phi}$, then one can state the joint multiphysics inverse problem for the inexact case as (compare equation (12))

$$\mathbf{s}\left(\widehat{\mathbf{m}}^{(1)}, \widehat{\mathbf{m}}^{(2)}\right) = \left\| \begin{array}{c} \mathbf{d}_0^{(1)} - \mathbf{f}^{(1)}\left(\widehat{\mathbf{m}}^{(1)}\right) \\ \mathbf{d}_0^{(2)} - \mathbf{f}^{(2)}\left(\widehat{\mathbf{m}}^{(2)}\right) \end{array} \right\|^2_{\mathbf{C}_{\mathbf{dd}}^{-1}} + \left\| \Delta\phi\left(\widehat{\mathbf{m}}^{(1)}, \widehat{\mathbf{m}}^{(2)}\right) - \Delta\phi_0 \right\|^2_{\mathbf{C}_{\phi\phi}^{-1}} + \left\| \begin{array}{c} \widehat{\mathbf{m}}^{(1)} - \mathbf{m}_0^{(1)} \\ \widehat{\mathbf{m}}^{(2)} - \mathbf{m}_0^{(2)} \end{array} \right\|^2_{\mathbf{C}_{\mathbf{m_0 m_0}}^{-1}}. \tag{21}$$

An explicit solution to this equation is given in iterative form by

$$\hat{\mathbf{m}}_{k+1}^{(j)} = \hat{\mathbf{m}}_k^{(j)} + \mathbf{H}_k^{-1}\mathbf{r}_k^{(j)} \quad j = 1, 2, \tag{22}$$

where

$$\mathbf{H}_k = \begin{bmatrix} \mathbf{A}_k^{(1)^T}\mathbf{C}_{dd}^{(1)^{-1}}\mathbf{A}_k^{(1)} + \mathbf{B}_k^{(1)^T}\mathbf{C}_{\phi\phi}^{-1}\mathbf{B}_k^{(1)} + \left(\mathbf{C}_{m_0 m_0}^{(1)}\right)^{-1} & -\mathbf{B}_k^{(1)^T}\mathbf{C}_{\phi\phi}^{-1}\mathbf{B}_k^{(2)} \\ -\mathbf{B}_k^{(2)^T}\mathbf{C}_{\phi\phi}^{-1}\mathbf{B}_k^{(1)} & \mathbf{A}_k^{(2)^T}\mathbf{C}_{dd}^{(2)^{-1}}\mathbf{A}_k^{(2)} + \mathbf{B}_k^{(2)^T}\mathbf{C}_{\phi\phi}^{-1}\mathbf{B}_k^{(2)} + \left(\mathbf{C}_{m_0 m_0}^{(2)}\right)^{-1} \end{bmatrix} \tag{23}$$

and

$$\mathbf{r}_k^{(j)} = \mathbf{A}_k^{(j)^T}\mathbf{C}_{dd}^{(j)^{-1}}\left(\mathbf{d}_0^{(j)} - \mathbf{f}^{(j)}\left(\hat{\mathbf{m}}_k^{(j)}\right)\right) + \mathbf{B}_k^{(j)^T}\mathbf{C}_{\phi\phi}^{-1} \cdot \left(\Delta\phi_0 - \Delta\phi\left(\widehat{\mathbf{m}}_k^{(1)}, \widehat{\mathbf{m}}_k^{(2)}\right)\right) + \left(\mathbf{C}_{m_0 m_0}^{(j)}\right)^{-1} \cdot \left(\mathbf{m}_0^{(j)} - \mathbf{m}_k^{(j)}\right). \tag{24}$$

Here, the derivation of the Hessian matrix $\mathbf{H}_k$ is based upon the Gauss-Newton inversion iteration. In this solution approach, the structural coupling terms are included in the off-diagonal elements of the Hessian matrix $\mathbf{H}_k$ (which is required to be full rank). Any redundancy or incompatibility in the structural measure is regarded as evidence of the inaccuracy of the function and should ideally be accounted for in the associated covariance matrix $\mathbf{C}_{\phi\phi}$. Conceptually, this objective function is identical to that given by equation (12) when $\mathbf{C}_{\phi\phi}^{-1} = \alpha\mathbf{I}$ and $\alpha \to \infty$, and the term on the right-hand side containing the observables $\mathbf{f}(\mathbf{m})$ are augmented with the regularization terms ($\mathbf{Dm}$) as in (12). However, computational differences can make equation (22) more suitable to inverse problems with special requirements. For example, in large-scale 3-D multiphysics imaging problems, it may be desirable to use the nonlinear conjugate gradients method in the minimization process. This method is linear convergent and relies on gradient information on the objective function and not its Hessian. Therefore, it can be readily applied to equation (22) but not to either equation (14) or (23).

[21] *Tryggvason and Linde* [2006] minimize a quadratic objective function that determines model perturbations from a background model, and the minimization of the cross-gradient constraint seeks to encourage structural resemblance within the model perturbations rather than the actual physical property fields (seismic compressional-wave velocity, Vp and shear wave velocity, Vs). Their objective function is similar to equation (21) but formulated in terms of model perturbations for Vp and Vs $\left(\Delta\mathbf{m} = \begin{bmatrix} \Delta\mathbf{m}^{\mathrm{P}} \\ \Delta\mathbf{m}^{\mathrm{S}} \end{bmatrix}\right)$. After linearization of the travel time equation, their resulting system of equations to solve is

$$\begin{bmatrix} \mathbf{A} \\ \alpha\mathbf{D} \\ \lambda\mathbf{B} \end{bmatrix} [\Delta\mathbf{m}] = \begin{bmatrix} \Delta\mathbf{d} \\ 0 \\ -\lambda\tau \end{bmatrix}, \tag{25}$$

where $\Delta\mathbf{d}$ and $\mathbf{A}$ are the travel times and their partial derivatives with respect to the slowness (reciprocal of velocity) parameters. $\mathbf{D}$ is a Laplacian operator used to control the roughness of the slowness perturbation field and α is the regularization parameter. $\mathbf{B}$ is the matrix of partial derivatives of the cross-gradient function (τ) with respect to the model parameters and λ is a constant weighting factor chosen heuristically. The system of equations is solved in a least squares sense using a nonlinear conjugate gradient method. This is an attractive approach for large-scale multiphysics inverse problems. *Linde et al.* [2006, 2008] adopt a similar approach

and present an equivalent equation to (25). Their objective function at the k+1 iteration is basically equivalent to

$$\mathbf{s}\left(\widehat{\mathbf{m}}_{\mathbf{k}+1}^{(1)}, \widehat{\mathbf{m}}_{\mathbf{k}+1}^{(2)}\right) = \left\| \begin{matrix} \mathbf{d}_0^{(1)} - \left[\mathbf{f}^{(1)}\left(\widehat{\mathbf{m}}_{\mathbf{k}}^{(1)}\right) + \mathbf{A}_{\mathbf{k}}^{(1)}\left(\widehat{\mathbf{m}}_{\mathbf{k}+1}^{(1)} - \widehat{\mathbf{m}}_{\mathbf{k}}^{(1)}\right)\right] \\ \mathbf{d}_0^{(2)} - \left[\mathbf{f}^{(2)}\left(\widehat{\mathbf{m}}_{\mathbf{k}}^{(2)}\right) + \mathbf{A}_{\mathbf{k}}^{(2)}\left(\widehat{\mathbf{m}}_{\mathbf{k}+1}^{(2)} - \widehat{\mathbf{m}}_{\mathbf{k}}^{(2)}\right)\right] \end{matrix} \right\|_{\mathbf{C}_{dd}^{-1}}^2 + \left\| \begin{matrix} \widehat{\mathbf{m}}_{\mathbf{k}+1}^{(1)} - \mathbf{m}_0^{(1)} \\ \widehat{\mathbf{m}}_{\mathbf{k}+1}^{(2)} - \mathbf{m}_0^{(2)} \end{matrix} \right\|_{\mathbf{c}_{\phi\phi}^{-1}}^2 + \lambda^2 \left\| \Delta\phi\left(\widehat{\mathbf{m}}_{\mathbf{k}}^{(1)}, \widehat{\mathbf{m}}_{\mathbf{k}}^{(2)}\right) + \mathbf{B}_{\mathbf{k}}^{(1)}\left(\widehat{\mathbf{m}}_{\mathbf{k}+1}^{(1)} - \widehat{\mathbf{m}}_{\mathbf{k}}^{(1)}\right) + \mathbf{B}_{\mathbf{k}}^{(2)}\left(\widehat{\mathbf{m}}_{\mathbf{k}+1}^{(2)} - \widehat{\mathbf{m}}_{\mathbf{k}}^{(2)}\right) \right\|^2, \tag{26}$$

where $\Delta\phi(\hat{\mathbf{m}}_i^{(1)}, \hat{\mathbf{m}}_i^{(2)}) = \tau(\hat{\mathbf{m}}_i^{(1)}, \hat{\mathbf{m}}_i^{(2)})$, $\mathbf{B}_k$ is the Jacobian matrix associated with the cross-gradient function and λ is a weighting factor. A particular choice of *Linde et al.* [2006, 2008] is to set λ large enough so as to mimic an exact structural resemblance approach. A conjugate gradient method was used to solve the problem and they have shown successful results of joint 3-D inversion of electrical resistivity and cross-hole georadar and seismic data.

[22] *Hu et al.* [2009] propose an alternative joint multiphysics inversion approach with inexact structural constraints. Their objective function may be generally stated as finding the updated seismic and electromagnetic model models ($\widehat{\mathbf{m}}_{k+1}^{(1)}$, $\widehat{\mathbf{m}}_{k+1}^{(2)}$) that minimize

$$s\left(\widehat{\mathbf{m}}_{k+1}^{(1)}, \widehat{\mathbf{m}}_{k+1}^{(2)}\right) = \left\| \begin{matrix} \mathbf{d}_0^{(1)} - \mathbf{f}^{(1)}\left(\widehat{\mathbf{m}}_{k+1}^{(1)}\right) \\ \mathbf{d}_0^{(2)} - \mathbf{f}^{(2)}\left(\widehat{\mathbf{m}}_{k+1}^{(2)}\right) \end{matrix} \right\|_{\mathbf{C}_{dd}^{-1}}^2 + \left\| \begin{matrix} \mathbf{D}\,\widehat{\mathbf{m}}_{k+1}^{(1)} \\ \mathbf{D}\,\widehat{\mathbf{m}}_{k+1}^{(2)} \end{matrix} \right\|_{\mathbf{C}_{DD}^{-1}}^2 + \left\| \begin{matrix} \mathbf{B}_k^{(1)}\,\widehat{\mathbf{m}}_{k+1}^{(1)} \\ \mathbf{B}_k^{(2)}\,\widehat{\mathbf{m}}_{k+1}^{(2)} \end{matrix} \right\|_{\mathbf{C}_{\phi\phi}^{-1}}^2. \tag{27}$$

As in the previous formulations, their weighting covariance matrices are all diagonal (i.e., no implicit cross correlation). The structural constraint in equation (27) is notably different from that of equation (26). The least squares normal equations derived from equation (27) have two fundamental differences from those given in equations (23) and (24). First, the corresponding Hessian matrix $\mathbf{H}_k$ lacks the cross-correlating block term $\mathbf{B}_k^{(1)T}\mathbf{C}_{\phi\phi}^{-1}\mathbf{B}_k^{(2)}$ present in (23). This fully decouples the solution of equation (27) into two separate minimization problems that make the problem less computationally expensive but at the cost of loosing valuable cross-correlating terms. Second, the corresponding gradient vector (compare equation (24)) lacks the structural resemblance term $\mathbf{B}_k^{(j)T}\mathbf{C}_{\phi\phi}^{-1}(\Delta\phi(\widehat{\mathbf{m}}_k^{(1)}, \widehat{\mathbf{m}}_k^{(2)}))$. This effectively makes the updated models at iteration k+1 ($\hat{\mathbf{m}}_{k+1}$) insensitive to the mutual structural dissimilarities $\Delta\phi(\widehat{\mathbf{m}}_k^{(1)}, \widehat{\mathbf{m}}_k^{(2)})$ borne by their predecessors ($\hat{\mathbf{m}}_k$). The combined effect is that the cross-gradient function may never attain values close enough to zero unless one of the property gradients becomes zero itself. We therefore think that there is no compelling argument in favor of using this approach.

3.3. Joint Inversion With Direction-Independent Structural Constraints

[23] There are a few joint inversion approaches that disregard the actual direction of the property changes despite its wide use in image processing as an edge detector [e.g., *Parker*, 1997] and indicator of even the actual magnitude of property changes. In this field, *Haber and Oldenburg* [1997] and *Zhang and Morgan* [1997] proposed independently the use of normalized versions of Laplacian operators ($\phi = \kappa\nabla^2 m$) as measures of image morphology and specifically the edges of objects present in the images (equations (8) and (9)). *Haber and Oldenburg* [1997] define the objective function as minimizing

$$s\left(\widehat{\mathbf{m}}^{(1)}, \widehat{\mathbf{m}}^{(2)}\right) = \left\| \begin{matrix} \mathbf{d}_0^{(1)} - \mathbf{f}^{(1)}\left(\widehat{\mathbf{m}}^{(1)}\right) \\ \mathbf{d}_0^{(2)} - \mathbf{f}^{(2)}\left(\widehat{\mathbf{m}}^{(2)}\right) \end{matrix} \right\|_{\mu}^2 + \left\| \phi\left(\widehat{\mathbf{m}}^{(1)}\right) - \phi\left(\widehat{\mathbf{m}}^{(2)}\right) \right\|^2, \tag{28}$$

where the structural measure ϕ is defined in equation (8) and μ is a weighting factor that controls the trade-off between structural difference and data misfit. The functions $\mathbf{f}^{(j)}$ are linearized and the equation solved iteratively using Krylov space techniques. In contrast to the previously described approaches, this particular scheme cannot emulate an exact resemblance approach as the damping factor μ cannot be restricted to a large value and must be designed experimentally. The problems of convergence and local minima are partially alleviated by restricting the step size in the iteration by adding an extra term and damping factor, $\xi\|\delta\mathbf{m}\|^2$ in the objective function. In this case the selection of both μ and ξ is done using different approaches. The procedure of stepwise length control resembles the data weighting relaxation used by the other approaches. *Zhang and Morgan* [1997] propose an objective function that closely resembles equation (28). In their case, the corresponding structure curvatures are normalized by the average values of the Laplacian operator across each image. This normalizing factor must be chosen based on a previous estimate of the models in order to conserve the linearity of the structural measure.

3.4. Uncertainty Analysis in Structure-Coupled Multiphysics Imaging

[24] Although one can quickly appraise the solution to a given joint inverse problem by examining the cross-gradients function [e.g., see *Gallardo and Meju*, 2007], to quantify the quality of the parameters estimated by joint multiphysical inversion, the full covariance information or bounding solutions must be determined. The standard uncoupled least squares solution $\widehat{\mathbf{m}}_{\mathrm{LS}} = \begin{bmatrix} \widehat{\mathbf{m}}_{\mathrm{LS}}^{(1)} \\ \widehat{\mathbf{m}}_{\mathrm{LS}}^{(2)} \end{bmatrix}$ that is an update of a previous model estimate $\widehat{\mathbf{m}}_k = \begin{bmatrix} \widehat{\mathbf{m}}_k^{(1)} \\ \widehat{\mathbf{m}}_k^{(2)} \end{bmatrix}$ can be expressed as (compare equation (13))

$$\widehat{\mathbf{m}}_{\mathrm{LS}} = \widehat{\mathbf{m}}_k + \mathbf{N}_k^{-1}\mathbf{n}_k, \tag{29}$$

where $\mathbf{N}_k$ and $\mathbf{n}_k$ are given by equations (14) and (15), respectively. Note that in this expression, all the random variables are associated with the vector $\mathbf{n}_k$ (see equation (15)). The estimator $\widehat{\mathbf{m}}_{k+1}$ of the structurally coupled models given in equation (13) may then be compactly expressed as

$$\widehat{\mathbf{m}}_{k+1} = \widehat{\mathbf{m}}_{\mathrm{LS}} - \mathbf{N}_k^{-1}\mathbf{B}_k^T\left(\mathbf{B}_k\mathbf{N}_k^{-1}\mathbf{B}_k^T\right)^{-1}\left\{\mathbf{B}_k\mathbf{N}_k^{-1}\mathbf{n}_k + \Delta\phi(\widehat{\mathbf{m}}_k)\right\}. \tag{30}$$

[25] Since $\widehat{\mathbf{m}}_{k+1}$ depends on observable data which are assumed to be random variables, this estimate is itself a random variable. We can then calculate the mathematical expectation of this estimate as

$$E(\widehat{\mathbf{m}}_{k+1}) = E(\widehat{\mathbf{m}}_{\mathrm{LS}}) - \mathbf{N}_k^{-1}\mathbf{B}_k^T\left(\mathbf{B}_k\mathbf{N}_k^{-1}\mathbf{B}_k^T\right)^{-1} \cdot \left\{\mathbf{B}_k\mathbf{N}_k^{-1}E(\mathbf{n}_k) + E(\Delta\phi(\widehat{\mathbf{m}}_k))\right\}. \tag{31}$$

Hence, it is easy to show that $E(\widehat{\mathbf{m}}_{k+1}) = E(\widehat{\mathbf{m}}_{\mathrm{LS}})$ if the following two conditions are satisfied:

[26] (1) $E(\mathbf{d}_0 - \mathbf{f}(\widehat{\mathbf{m}}_k)) = \mathbf{0}$, i.e., if model predictions and observation errors do not show a systematic bias, for instance, due to incorrect assumptions of model dimensionality, incompatible parameterizations or unpredicted systematic effects in the data. This estimation bias remains not only in the $E(\widehat{\mathbf{m}}_{\mathrm{LS}})$ term but also as a propagated structural uncertainty in the reconstructed images given by the quantity $-\mathbf{N}^{-1}\,\mathbf{B}^T(\mathbf{B}\mathbf{N}^{-1}\,\mathbf{B}^T)^{-1}\,\mathbf{B}\mathbf{N}^{-1}\,\mathbf{A}^T\,\mathbf{C}_{dd}^{-1}E(\mathbf{d} - \mathbf{f}(\widehat{\mathbf{m}}_k))$.

[27] (2) $E(\Delta\phi(\widehat{\mathbf{m}}_k)) = 0$. This condition relates to the accuracy of $\Delta\phi$ as a measure of common structure.

[28] Once these two conditions are satisfied, it can be demonstrated that $E(\widehat{\mathbf{m}}_{k+1}) = \mathbf{m}$ only when the estimator $E(\widehat{\mathbf{m}}_{\mathrm{LS}}) = \mathbf{m}$, i.e., when the least squares estimator is unbiased.

[29] Statistically, the covariance matrix of the joint inversion estimator is defined as

$$\mathbf{C}_{\hat{\mathbf{m}}\hat{\mathbf{m}}} = E[(\hat{\mathbf{m}}_{k+1} - E(\hat{\mathbf{m}}_{k+1}))][(\hat{\mathbf{m}}_{k+1} - E(\hat{\mathbf{m}}_{k+1}))]^T. \tag{32}$$

If

$$\widehat{\mathbf{m}}_{k+1} = \widehat{\mathbf{m}}_k + \mathbf{N}_k^{-1}\mathbf{n}_k - \mathbf{P}_k\left\{\mathbf{B}_k\mathbf{N}_k^{-1}\mathbf{n}_k + \Delta\phi(\widehat{\mathbf{m}}_k)\right\} \tag{33}$$

and

$$\mathbf{P}_k = \left(\mathbf{B}_k\mathbf{N}_k^{-1}\mathbf{B}_k^T\right)^{-1}, \tag{34}$$

then

$$\begin{aligned}\widehat{\mathbf{m}}_{k+1} - E(\widehat{\mathbf{m}}_{k+1}) = {} & [\widehat{\mathbf{m}}_k - E(\widehat{\mathbf{m}}_k)] \\ & + \left(\mathbf{N}_k^{-1} - \mathbf{N}_k^{-1}\mathbf{B}_k^T\mathbf{P}_k\mathbf{B}_k^T\mathbf{N}_k^{-1}\right)[\mathbf{n}_k - E(\mathbf{n}_k)] \\ & - \mathbf{P}_k[\Delta\phi(\widehat{\mathbf{m}}_k) - E(\Delta\phi(\widehat{\mathbf{m}}_k))].\end{aligned} \tag{35}$$

The direct application of equation (32) will require good estimates of the covariance matrix of the previous model or iterate, and the mutual cross-coupling of these two estimates and actual experimental data. Unfortunately all these estimates will be generally unavailable. Instead, we may consider that the previous model serves only as a fixed reference point and hence assume that $E(\widehat{\mathbf{m}}_k) = \widehat{\mathbf{m}}_k$ and $\mathbf{E}(\mathbf{t}(\widehat{\mathbf{m}}_k)) = \mathbf{t}(\widehat{\mathbf{m}}_k)$. Although it may be argued that this assumption may limit the role of the covariance matrix to a stability measure, it will be much easier to compute and will provide a useful preliminary insight into the uncertainty problem.

[30] Using equations (32)–(35), it is straightforward to show that

$$\mathbf{C}_{\hat{\mathbf{m}}\hat{\mathbf{m}}} = \mathbf{N}_k^{-1} - \mathbf{N}_k^{-1}\mathbf{B}_k^T\mathbf{P}_k\mathbf{B}_k\mathbf{N}_k^{-1}. \tag{36}$$

For comparison, if the same criterion is applied to the least squares estimator given by equation (35) then, the covariance of the joint estimator can be restated as

$$\mathbf{C}_{\hat{\mathbf{m}}\hat{\mathbf{m}}} = \mathbf{C}_{\hat{\mathbf{m}}\mathrm{LS}\hat{\mathbf{m}}\mathrm{LS}} - \mathbf{C}_{\hat{\mathbf{m}}\mathrm{LS}\hat{\mathbf{m}}\mathrm{LS}}\mathbf{B}_k^T\mathbf{P}_k\mathbf{B}_k\mathbf{C}_{\hat{\mathbf{m}}\mathrm{LS}\hat{\mathbf{m}}\mathrm{LS}}. \tag{37}$$

Since the second part of this expression is a positive semidefinite matrix, then the diagonal elements of $\mathbf{C}_{\hat{\mathbf{m}}\hat{\mathbf{m}}}$ will not be greater than those of $\mathbf{C}_{\hat{\mathbf{m}}\mathrm{LS}\hat{\mathbf{m}}\mathrm{LS}}$, which can be interpreted as an increased precision of the jointly estimated model parameters over the conventional separate estimations. Additionally, the off-diagonal blocks of the covariance matrix $\mathbf{C}_{\hat{\mathbf{m}}\hat{\mathbf{m}}}$ bear nonzero values that result in an intrinsic correlation between the parameters of different model representations given exclusively by the right hand terms of equation (37), i.e., by the common structure. It is notable that the correlation terms of equation (37) are intrinsically dependent on individual intraimage correlations from the least squares estimator $\mathbf{C}_{\hat{\mathbf{m}}\mathrm{LS}\hat{\mathbf{m}}\mathrm{LS}}$, which may be driven by both data and regularizing assumptions. The question here is, Is this simplified covariance estimation technique realistic for the typical large-scale inverse problems encountered in geophysical sciences?

[31] Equations (32)–(37) are based upon a linear analysis of a nonlinear problem, with additional simplifications that we introduced. Note that the inverse of the normal equations

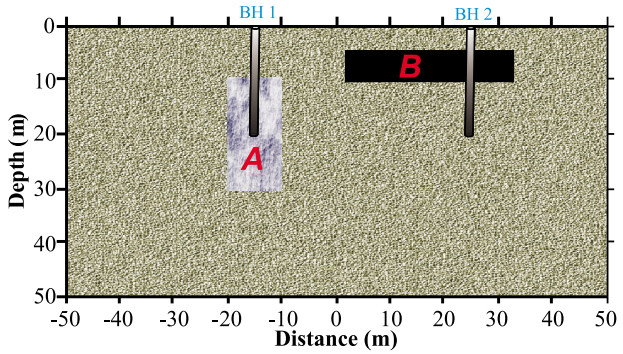

Lithotype	Density	Magnetization	Electrical resistivity
-1 (B)	-1.8	-0.2	10000
0 (Background)	0	0	100
+1 (A)	+0.3	+1.2	10

Figure 5. Test model used for the joint cross-gradients inversion of geophysical and lithological data. Two tabular bodies A and B are embedded in a homogeneous medium. Two boreholes BH1 and BH2 intersect these bodies. The schematic borehole sections show the lithological units that are conventionally qualitatively described. The tabulated numbers represent the assigned property values for the rock-type, density (g/cm^3), magnetization (A/m), and electrical resistivity (Ω.m) of the various geological units in the model.

matrix that carries the covariance information is very expensive to compute and hence a drawback when dealing with large-scale inverse problems. Consequently, these equations may only serve as metrics for simple model appraisal in small-size joint inverse problems. For large data sets, there is an increasing interest in the use of Monte Carlo integration methods for approximating large error covariance matrices especially in gravity field modeling, and facilitating the related error propagation computations [see, e.g., *Gundlich et al.*, 2003; *Alkhatib and Schuh*, 2007]. These methods can be easily adapted to large-scale structure-coupled inverse problems. As noted elsewhere in a different context [*Borovikov et al.*, 2005], an important advantage of Monte Carlo covariance estimation is that it will provide a natural way to estimate cross covariances between the fields of different physical variables that constitute the parameters of the structure-coupled models. The regularized extremal bounds analysis method [*Meju*, 2009] has been suggested for computing model bounds which are consistent with our measurement and modeling errors in nonlinear inversion, but this may be unfeasible for some large-scale joint inverse problems.

4. INTEGRATION OF PHYSICAL AND NONPHYSICAL INFORMATION

[32] Realistic integration of hard and soft (non-physics-based) constraints is a nontrivial mathematical challenge. In geophysical imaging, observational data on a physical system may include remote measurements on the surface of the Earth and in situ recordings within boreholes, as well as laboratory measurements on core samples taken at different depths in the boreholes and their nonnumerical geological descriptions. These data are thus heterogeneous and of multiple-spatial (i.e., micro- to macro-) scale in nature. Conventionally, geologic scenarios, seismic and petroleum production data are integrated using a probabilistic approach [*Caers et al.*, 2006]. Some workers [*Gallardo*, 2007b; *Lelièvre*, 2009; *Lelièvre and Oldenburg*, 2009] demonstrate that geological and geophysical data can also be integrated naturally in joint image reconstruction using a deterministic approach with much less computational burden. The exciting prospect here is the slowly emerging possibility of realistic structural and compositional classification of targets via deterministic or Bayesian structure-coupled joint inversion. In the Earth sciences, this will lead to improved prediction of rock physical properties relevant to fluid flow in subterranean reservoirs, if multiscale variations can be adequately accounted for as discussed in section 5.1.

[33] *Cardiff and Kitanidis* [2009] developed the equivalent Bayesian framework for gradient-based structural inversion and uncertainty analysis in hydrology. They propose a Bayesian inversion protocol, which permits the definition of different structural zones or *hydrofacies* locations using the level set method and for moving the boundaries between zones using a gradient-based technique that improves fit through iterative deformation of the boundaries. They demonstrate that the level set method is well suited for joint inversion problems and present a strategy for integrating different data types (such as hydrologic and geophysical) for simultaneous boundary delineation without assuming strict *petrophysical relationships*. Although the underlying philosophy in their probabilistic joint inversion approach is the same as in the cross-gradients method of *Gallardo and Meju* [2003, 2004], it is associated with a more significant computational overhead, especially in multidimensional space. The challenge is to incorporate lithological information into a multiphysics inversion algorithm within a deterministic framework.

[34] *Gallardo* [2007b] applied the cross-gradient technique to synthetic data consisting of remote geophysical observations and borehole geological data. The test model consists of a homogeneous medium in which are embedded two rectangular bodies (labeled A and B in Figure 5). Two 20 m deep boreholes (BH1 and BH2 in Figure 5) intersect these target bodies. BH1 permeates the upper part of body A whereas BH2 cuts across the entire thickness of body B. The various parts of the model are assigned coherent values of density, electrical resistivity and magnetization, while the assumed corresponding lithological units (*lithotypes* for short) are assigned integer numbers. To all the synthetic data were added normally distributed Gaussian errors with the respective standard deviations given in Table 1.

[35] *Gallardo* [2007b] inverted these synthetic data using a homogeneous initial model. Three different inversion experiments were run, namely, (1) Separate inversion of geophysical and lithotype data with no cross-gradient constraint, (2) joint inversion of the multiple geophysical data

TABLE 1. Standard Deviation of the Gaussian Noise Added to Each Data Set and Level of Misfit Achieved for Each of the Three Inversion Experiments[a]

Type of Inversion	Gravity σ = 2 (μGal)	Magnetics σ = 2 (nT)	Resistivity σ = 3(%)	Lithotype σ = 0.1 units
Separate inversion	RMS = 0.864	RMS = 0.742	RMS= 0.948	RMS = 0.927
Joint geophysical inversion	RMS = 0.881	RMS = 0.777	RMS = 1.031	-
Joint lithotype inversion	RMS = 0.890	RMS = 0.789	RMS = 1.077	RMS = 1.002

[a]The misfit is the normalized RMS value of the data residuals.

alone, yielding structurally coupled physical property distributions (density, magnetization and logarithm of electrical resistivity), and (3) joint inversion of all geophysical and synthetic lithotype data yielding four coupled property distributions. The final models obtained from the three inversion experiments are compared in Figure 6 and their statistical characteristics are summarized in Table 1. As shown in Table 1, they all produced models with appropriate data misfit, and marginal increments in the misfit are correlated to the increment in the number of jointly estimated images. Notice that the set of models found in each experiment show remarkable differences in structural resemblance. The images obtained from separate (i.e., single physics) inversion (Figures 6a–6d) show significant differences; the gravity and magnetic models reflect the lack of depth resolution and the lithotype model is affected by the complete lack of knowledge of what lithologies exist beyond the confines of the two boreholes. In the latter case, the lithotype values are extrapolated on the basis of the smoothness constraint, i.e., smeared in the model following mainly the extension of the known borehole/surface lithological evidence. These structural differences, as measured by the corresponding cross-gradient values for each pair of presented images, are listed in Table 2.

[36] The images obtained from structure-coupled multiphysics inversion are structurally compatible as shown by the distribution of the physical properties (Figures 6e–6g) and their significantly reduced cross-gradient values (Table 2). Gravity and magnetic models benefited significantly from, and adopted the structure contributed by, the electrical model. The images obtained from the joint geophysical and lithotype inversion (Figures 6h–6k) bear similar features to those seen in the purely multiphysical inversion experiment (Figures 6e–6g), but the region around the boreholes are now better constrained by the addition of lithotype data leading to higher model accuracy. However, the employed smoothness constraint is incompatible with the assumed sharp lithological constraints and resulted in the marginally larger cross-gradient values for this experiment than for the purely multiphysical experiment (see Table 2).

5. CHALLENGES, OPPORTUNITIES, AND FUTURE DIRECTIONS

[37] We have so far discussed the use of measures of common structure in the solution and integration of multiphysics images and the associated uncertainties. There are still hurdles to be scaled in the use of structural constraints for combining information from multiple images acquired with different devices and modalities. The outstanding conceptual, physical and computational challenges are in the areas of structural and compositional classification of physical reality (see section 2.3), integration of soft (non-physics-based) constraints such as geological information in joint multiphysics imaging (see section 4), multiscale modeling of heterogeneity or anisotropy and linkages to fluid flow phenomena, uncertainty quantification for large-scale systems (see section 3.4), and computational limitations. We will address the challenges posed by model complexity and computational issues next.

5.1. Complexity of Natural Physical Systems

[38] An important challenge in multiphysics imaging is how to make two or more geophysical property fields consistent if they have different scale lengths. For example, electrical conductivity and reflectivity arising from magnetotelluric and seismic measurements may differ significantly in scale length. *Gallardo et al.* [2010] applied the cross-gradient constraint in the joint inversion of seismic reflection, magnetotelluric, gravity and magnetic data from marine exploration for hydrocarbons. The seismic reflection data are the two-way travel times (TWT) picked for five selected reflectors in the seismic time section. The depths to these reflectors (floating reflectors) were estimated using average interval velocities as in conventional practice. For the cross-gradient joint resistivity and velocity inversion, a common inversion grid was selected for all the geophysical methods with dense sampling over the region of common data coverage. To allow for features of different scale length, the grid is resampled according to specific accuracy requirements for the seismic and magnetotelluric forward modeling and Jacobian computations. During the inversion process, the cross-gradient constrained MT conductivity and seismic velocity are estimated whereas the depths to the floating reflectors are treated as a priori information, consistent with equation (12). More research is needed along this line. Perhaps the most difficult challenge facing structure-coupled multiphysics inversion is how to model the complexity of most natural physical systems that form the subjects of investigation. While most biological bodies contain well-defined interfaces between different regions of tissue-types or anatomical material (i.e., essentially structured), the Earth system is rather structurally and compositionally complex. Consequently in Earth imaging, direct recovery of structural information from multiple physical measurements is fraught with uncertainty unless adequate attention is paid to issues such as anisotropy and heterogeneity, and their multiscale nature (i.e., ranging from microscale to mega scale). Although

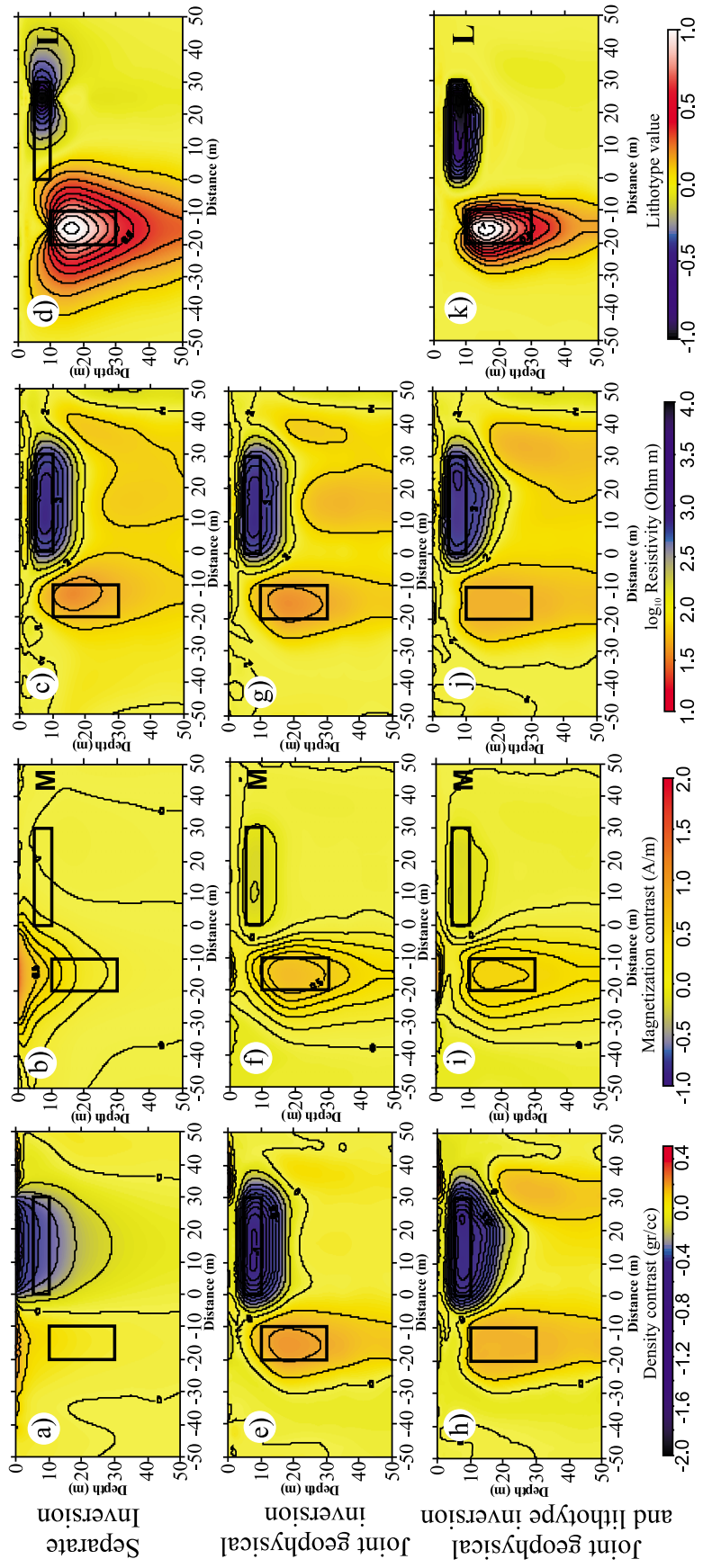

Figure 6. Results of the inversion of data from (a, e, h) gravity δ, (b, f, i) magnetic M, (c, g, j) resistivity ρ, and (d, k) borehole/surface lithological L synthetic experiments. Models at the top are obtained from separate data inversion. Models in middle row are from structure-coupled joint inversion of multiple geophysical data. Models in bottom row are from structure-coupled joint inversion of multiple geophysical and borehole lithological data (modified from *Gallardo* [2007b]).

TABLE 2. Summary of RMS Cross-Gradient Values for the Models Derived From Separate Inversion (in Parentheses), Joint Geophysical Inversion ($^{+}$), and Joint Geophysical and Borehole Data Inversion ($^{++}$)[a]

Cross-Gradient Values $\times 10^{-5}$	Gravity	Magnetics	Resistivity	Lithotype
Gravity	0	(173)	(386)	(212)
Magnetic	0.60^{+} 2.05^{++}	0	(254)	(152)
Resistivity	0.98^{+} 2.59^{++}	1.88^{+} 2.27^{++}	0	(276)
Lithotype	- 2.60^{++}	- 1.62^{++}	- 2.67^{++}	0

[a]Any combination of two images that are exactly the same have zero cross-gradient values. Note the significant reduction in cross-gradient values for the structurally coupled joint inversion models compared to the separately estimated models.

it is still argued whether heterogeneity and anisotropy are separable in gross Earth imaging, there has been an increasing awareness of complexity as an essential theoretical challenge in many important predictive modeling problems. Multiscale concepts are believed to provide a rational path for treating the errors associated with model limitations since they essentially provide a framework for information exchange between different representations of a physical phenomenon. Simultaneous execution of these operational representations of information will lead to better models of physical reality, relevant to improved multiphysics imaging.

[39] The complexity of natural physical systems also dictates that adequate system characterization must involve some combination of measurements of the electrical, mechanical and chemical (or fluid transport) properties of the bodies under investigation. In the geophysical sciences, the physics of fluid flow and electromagnetic induction or sound wave propagation phenomena in porous media can be coupled through fluid saturation equations [*Pride*, 1994; *Alpak et al.*, 2008]. Linkages between multiphysics imaging and fluid flow processes within materials in the Earth's crust are now emerging [e.g., *Cassiani and Binley*, 2005; *Linde et al.*, 2006; *Alpak et al.*, 2008; *Looms et al.*, 2008]. *Binley et al.* [2004] use a combined multidimensional georadar and electrical resistivity tomography to constrain moisture transport modeling for a relatively homogeneous sandstone material. *Binley et al.* [2004] generate realizations of 1-D geology (homogeneous sandstone) based on gamma logs and geostatistics of the geophysical data, then simulate hydrological models of the geology and compare against cross-hole georadar responses. *Cassiani and Binley* [2005] build on *Binley et al.* [2004] and try to link between hydrological and geophysical models for this relatively homogeneous sandstone material. *Linde et al.* [2006, 2008] use the results from joint multidimensional inversion of multiplatform geophysical measurements to constrain water flow modeling in sedimentary rocks occurring at shallow depth. *Looms et al.* [2008] run hydrological model of recharge and compare responses in an attempt to find the optimum hydrological parameters comparing against 3-D electrical resistivity tomography (ERT) and cross-hole georadar images. *Alpak et al.* [2008] use the result of combined multiphysical structural imaging to inform subsequent flow modeling of a petroleum system. What is now required is the simultaneous linkage of multiphysics structural imaging and flow or transport modeling in 3-D anisotropic media. We see this as the way forward and the ultimate challenge for any method of remote interrogation of complex systems such as the fluid-bearing regions within the Earth's crust. However, considerable computational resources will be required for realistic inverse modeling of such systems.

[40] An obvious application of 3-D joint anisotropic multiphysics and transport modeling will be in the important area of time-lapse characterization and monitoring of spatiotemporal changes in physiochemical systems. The idea that physical properties or state variables change with time is not new. In medical imaging, the study of temporal image series, the monitoring of time evolution of an agent injection, and treatment verification of preintervention and postintervention images are well established examples. In geophysical imaging of hydrocarbon reservoirs, the difference between data acquired at an initial survey (base data) and another set acquired in successive time periods (monitor data) is used routinely to show the location of water replacing oil which may be mapped across the field using controlled seismic sources [e.g., *Lumley*, 2001; *Calvert*, 2005; *Aarre*, 2006] or *electromagnetic methods* (Italicized terms are defined in the glossary, after the main text.) [*Orange et al.*, 2009]. In geohydrolology, infiltration experiments or specially injected tracers are tracked in space and time, allowing the characterization of the properties of the subterranean transport media [*Binley et al.*, 2004]. In biological imaging, soil water extraction by plant roots, the movement of sap in tree trunks and the development of root mass in the subsoil have been monitored using physics-based approach. In all these fields, volumetrically significant movement of fluids may occur on length scales below that of the resolution and noise threshold allowed by an individual physical data set such that any inferences are subject to uncertainty. Combining multiple physical measurements of different modalities may be a better approach. For example, there are significant uncertainties in the quantitative analysis of only time-lapse seismic measurements over petroleum reservoirs [*Landrø*, 2002; *Furtney and Woods*, 2006; *Tsuneyama and Mavko*, 2007]. Yet it is observed that fluid withdrawal from a reservoir may be associated with geomechanical deformations (especially in weak rock formations) and seismic time shifts [e.g., *Minkoff et al.*, 2004; *Hatchell and Bourne*, 2005; *Aarre*, 2006; *Rickett et al.*, 2007]. An established physical method for imaging or monitoring subterranean fluid flow processes is the spontaneous polarization method [e.g., *Kemna et al.*, 2004], and changes in reservoir porosity, pressure and fluid saturation computed using coupled fluid flow and geomechanical deformation modeling can be used to determine changes in density and seismic velocities with time [*Minkoff et al.*, 2004]. It is thus logical to expect that fully coupled 3-D fluid flow and geomechanical deformation simulations and seismic modeling, linked with spontaneous potential and/or induced polarization modeling using the cross-gradients approach, would be a useful way forward in time-lapse

analysis. However, this would be fraught with significant computational difficulties.

5.2. Computational Issues

[41] What strategies might be adopted to overcome some of the computational challenges faced in joint multiphysics inversion? The gradient-based structurally coupled 3-D multimodal imaging approach is computationally intensive since it requires the full sensitivity matrix for each physical method. It can be implemented using direct matrix inversion techniques [*Haber and Oldenburg*, 1997; *Gallardo and Meju*, 2003; 2004; 2007; *Fregoso and Gallardo*, 2009] or a conjugate gradient approach [*Haber and Oldenburg*, 1997; *Tryggvason and Linde*, 2006]. The required sensitivities can be efficiently computed using reciprocity or adjoint state methods [e.g., *Kravaris and Seinfeld*, 1985; *Norton*, 1999; *Cirpka and Kitanidis*, 2000; *Rodi and Mackie*, 2001; *Shin et al.*, 2001; *Meyer et al.*, 2006; *Commer and Newman*, 2008]. The key challenge here is to make modifications to reduce the number of predictive or forward modeling calculations to a reasonable level during the computation of sensitivities. A simple way to get around this computational difficulty for the electrical method of geophysics, for example, is to initiate the inversion using a homogeneous half-space for which the sensitivity can be obtained analytically, use this in the first two iterations, then compute the rigorous sensitivity matrix at the third iteration and update it thereafter using the Broyden's technique [*Dennis and Schnabel*, 1996] as given by *Sasaki* [2004]. Another strategy to adopt might be the data space method of *Siripunvaraporn et al.* [2005]. The adjoint state method is emerging as the technique of choice in large-scale imaging [e.g., *Meyer et al.*, 2006; *Commer and Newman*, 2008] since, for n measurements, the determination of the sensitivity matrix requires the solution of only one forward problem and n adjoint problems that are similar to the forward problem. Another important consideration is that the size of numerical calculation will dramatically increase if realistic structures are to be modeled in 3-D; it is therefore better to parallelize the code to take advantage of modern computer architecture and to use a conjugate gradients approach. For example, *Commer and Newman* [2008] in their inversion of only electromagnetic data from an oil exploration survey required 200 million field unknowns in predictive modeling (forward problem) and imaging grids 400 nodes on a side. They implemented two levels of parallelization, in model space (requiring separate forward simulation and inversion grids) and in data space (requiring independent forward calculation of each transmitter-receiver set). Their imaging scheme was successfully tested on multiple distributed computing systems (10–32,766 processors).

[42] For any realistic large-scale joint seismic and electromagnetic imaging with associated fluid flow modeling as would obtain in energy resource and environmental applications, there will be a requirement for high levels of computational efficiency (tailored separate grids for forward and inverse modeling with potential for significant solution acceleration; adjoint state method of sensitivity calculation) and several thousands of processors. The conjugate gradients method may be the method of choice when rapid convergence toward a good data fit is desired. However, like all approximate subspace methods, no robust estimates of model uncertainty are readily available for 3-D multiphysics inverse problems using this approach. Direct matrix inversion provides the possibility to obtain covariance and resolution matrices but have been attempted for small-scale single-physics imaging [*Alumbaugh and Newman*, 2000]. Present-day computational resources will allow full inversion methods such as the singular value decomposition method [e.g., *Kalscheuer and Pedersen*, 2007; *Kalscheuer et al.*, 2010] to be applied to some problems with more than 10000 unknowns to obtain covariance and resolution matrices. An important step forward in multiphysics data imaging would thus be to develop direct 3-D joint inversion techniques to obtain more mathematically rigorous estimates of model parameter uncertainty or resolution for problems with millions of unknowns. However, given the large-scale needs of the Earth science community, a Monte Carlo covariance estimation strategy [e.g., *Borovikov et al.*, 2005; *Alkhatib and Schuh*, 2007] would seem to be the most attractive way forward.

6. SUMMARY AND CONCLUSIONS

[43] It is well known in science and engineering that all indirect inference of system parameters and states based on finite observations is subject to uncertainty. The mathematical models describing the physical processes underlying the inference are oversimplified approximations of reality. The inverted experimental observations are of limited measurement accuracy. The typical physical system, such as the Earth, is complex and multiscale in nature. The constituent multiscale features have an aggregate effect on the measured multiphysics responses that are difficult or impossible to resolve, especially when inference is based on parameter estimates from individual physical fields. Accordingly, the issues of combined multiphysics parameter estimation and uncertainty quantification are recognized as critical elements necessary for continued advancement in imaging science. Significant progress has been made in recent years in the solution of geophysical imaging problems, and this review is devoted to the emerging techniques for the direct recovery of structural information from measured data using a generalized coupling based on structural gradients of the physical property fields. The underlying philosophy in multiphysics structure-coupled imaging is that the data sets, though disparate, should have features in common because they sense or reflect the same geological structure. Structural similarity between the multiple physical property distributions is achieved by imposing the constraint that the cross-product of the gradients of the property fields should be zero at structural boundaries for a given geological frame of reference. This can be formulated mathematically through the model gradients by requiring the cross-product of the model gradients to approach zero everywhere.

[44] In conclusion, the important feature of the structure-coupled inversion approach is that it allows direct recovery of structural information from physical data taken from different measurement platforms or modalities that may or may not be phenomenologically related. It is now possible to perform joint inversion wherever two or more physically measured data sets are available, and the relevant parameters are controlled by the same structure or state variables of the physical system being investigated. The inverse problems that are solved in joint inversion are much larger than for single-physics-based imaging. These can be handled to a large extent by the currently available computational resources, especially for small-scale problems. However, to fully exploit the system information in joint inversion, appropriate methods for quantifying model parameter reliability are desirable. We discussed some emerging metrics for assessing model uncertainty but suggest that further work needs to be done in this important area of research. Also in recent years, there has been an increasing awareness of complexity as an essential theoretical challenge in many important predictive modeling problems, and we expect 3-D anisotropic or multiscale modeling to become an integral part of large-scale multiphysics imaging in the next 5–10 years. There are some practical computational considerations that are necessary in large-scale structure-coupled 3-D multiphysics inverse modeling. Since this process requires 3-D forward modeling and imaging solutions, parallelization in the model and data spaces is necessary. The multilevel parallelization should be tailored to suit the attendant multiphysics forward simulation processes and the heterogeneous multicomponent data sets to be inverted, thus allowing for realistic imaging. Separation and optimization of the simulation and inversion grids will be essential, especially for joint 3-D full waveform seismic and electromagnetic imaging, and have potential for significant solution acceleration. It is anticipated that there will be several improvements in large-scale 3-D multiphysics imaging over the next 2–5 years because of the present high interest from the energy industry. We expect a massive increase in measured data volumes from 3-D coincident multicomponent seismic and electromagnetic surveys offshore. The large seismic and electromagnetic data and imaging volumes would require at least 10–100 times the present computing resources. We predict that the future availability of robust joint 3-D full waveform seismic and electromagnetic imaging coupled with fluid flow modeling will revolutionize resource exploration and development, especially in the energy industry.

GLOSSARY

Electrical resistivity method: measures the ability of Earth materials to impede the flow of galvanic currents passed through the materials. The actual physical property measured is electrical resistivity (SI units are ohm.m). The reciprocal is electrical conductivity (SI units are Siemens/m).

Electromagnetic methods: measure the ability of Earth materials to pass current when inductively energized. The actual physical property measured is electrical conductivity.

Cross-hole imaging: the art of reconstructing physical property fields in the region between boreholes using data furnished by sources and sensors that are systematically located in different boreholes.

Formation factor (F): a measure of the reduction in electrical conductivity due to the addition of an insulating phase to an electrolyte. $F = \sigma_w/\sigma_b$, where σ_w is the electrolyte conductivity and σ_b is the bulk rock conductivity.

Hydrofacies: a concept used to describe types or classes of groundwater with characteristic chemical compositions.

Geophysical well logging methods: measure variations in physical properties of rock down a borehole. These are adaptations of methods used on the surface of the Earth. The common ones are gamma ray, density, temperature, resistivity and sonic logging.

Georadar or ground-penetrating radar (GPR) method: records high-frequency electromagnetic waves transmitted and reflected from interfaces of contrasting dielectric permittivity.

Gravity method: measures spatial variations in the Earth's gravitational field caused by bodies of different densities. Physical property measured is density (SI units are Kg/m^3).

Lithology: a geological term for rock-type or stratigraphic units.

Lithofacies: a mappable subdivision of a stratigraphic unit that can be distinguished from adjacent subdivisions by its facies or lithologic features such as grain size, texture, mineralogy, and environment of formation.

Lithotype: a geological unit characterized by its specific lithology, depositional environment and climatic-stratigraphic position.

Magnetic method: measures spatial variations in the Earth's magnetic field caused by bodies of different magnetizations. Physical property measured is magnetic susceptibility which is the degree of magnetization of a material in response to an applied electric field.

Petrophysical relations: established correlations between rock-physical properties (such as porosity and water saturation) and the measurable geophysical signatures (such as electrical resistivity and sound wave velocity).

Seismic methods: measure spatial variations in the speed of propagation of sound waves through the Earth, commonly in the form of energy refraction or reflection at interfaces. Velocity and attenuation of elastic waves in Earth materials can be inferred from remote measurements. Two common seismic velocities used in imaging are compressional wave velocity (Vp) and shear wave velocity (Vs). The motion of a compressional wave is in the same direction as the wave propagation.

[45] **ACKNOWLEDGMENTS.** The motivation for this review resulted from the recently growing number of specialized workshops on joint geophysical inversion where issues of data fusion, uncertainty quantification, and validation of model predictions were addressed. We acknowledge the insightful discussions with N. Linde, A. Binley, G. Newman, and J. Harris, which helped shape this manuscript. Ideas from R. Ghanem of University of

Southern California helped shape section 2.2. We are grateful to reviewer 1 and reviewer 2 for their constructive comments which greatly improved the clarity of this paper.

[46] The Editor on this manuscript was Mark Moldwin. He thanks two anonymous reviewers.

REFERENCES

Aarre, V. (2006), Estimating 4D velocity changes and contact movement on the Norne field, *SEG Expanded Abstr.*, 3115–3119, doi: 10.1190/1.2370175.

Alkhatib, H., and W.-D. Schuh (2007), Integration of the Monte Carlo covariance estimation strategy into tailored solution procedures for large-scale least squares problems, *J. Geod.*, *81*, 53–66, doi:10.1007/s00190-006-0034-z.

Alpak, F. O., C. Torres-Verdin, and T. M. Habashy (2004), Joint inversion of transient pressure and dc resistivity measurements acquired with in-situ permanent sensors: A numerical study, *Geophysics*, *69*, 1173–1191, doi:10.1190/1.1801935.

Alpak, F. O., C. Torres-Verdin, and T. M. Habashy (2008), Estimation of in-situ petrophysical properties from wireline formation tester and induction logging measurements: A joint inversion approach, *J. Petrol. Sci. Eng.*, *63*, 1–17, doi:10.1016/j.petrol.2008.05.007.

Alumbaugh, D. L., and G. A. Newman (2000), Image appraisal for 2-D and 3-D electromagnetic inversion, *Geophysics*, *65*, 1455–1467, doi:10.1190/1.1444834.

Beckwith, C. W., and J. Baird (2001), Effect of biogenic gas bubbles on water flow through poorly decomposed blanket peat, *Water Resour. Res.*, *37*, 551–558, doi:10.1029/2000WR900303.

Bedrosian, P. A. (2007), MT+, integrating magnetotellurics to determine Earth structure, physical state, and processes, *Surv. Geophys.*, *28*(2–3), 121–167, doi:10.1007/s10712-007-9019-6.

Bedrosian, P. A., N. Maercklin, U. Weckmann, Y. Bartov, T. Ryberg, and O. Ritter (2007), Lithology-derived structure classification from the joint interpretation of magnetotelluric and seismic models, *Geophys. J. Int.*, *170*(2), 737–748, doi:10.1111/j.1365-246X.2007.03440.x.

Berge, P. A., J. G. Berryman, H. Bertete-Aguirre, P. Bonner, J. J. Roberts, and D. Wildenschild (2000), Joint inversion of geophysical data for site characterization and restoration monitoring, *Rep. LLNL UCRL-ID-128343*, U.S. Dep. of Energy, Washington, D. C.

Bergman, B., A. Tryggvason, and C. Juhlin (2004), High-resolution seismic traveltime tomography incorporating static corrections applied to a till-covered bedrock environment, *Geophysics*, *69*, 1082–1090, doi:10.1190/1.1778250.

Binley, A., P. Winship, L. J. West, M. Pokar, and R. Middleton (2002), Seasonal variation of moisture content in unsaturated sandstone inferred from borehole radar and resistivity profiles, *J. Hydrol.*, *267*, 160–172, doi:10.1016/S0022-1694(02)00147-6.

Binley, A., G. Cassiani, and P. Winship (2004), Characterization of heterogeneity in unsaturated sandstone using borehole logs and cross-borehole tomography, in *Aquifer Characterization*, vol. 80, edited by J. Bridge and D. Hyndman, pp. 129–138, Soc. for Sediment. Geol., Tulsa, Okla.

Borovikov, A., M. M. Rienecker, C. L. Keppenne, and G. C. Johnson (2005), Multivariate error covariance estimates by Monte Carlo simulation and assimilation studies in the Pacific Ocean, *Mon. Weather Rev.*, *133*, 2310–2334, doi:10.1175/MWR2984.1.

Bosch, M. (1999), Lithologic tomography: From plural geophysical data to lithology estimation, *J. Geophys. Res.*, *104*(B1), 749–766, doi:10.1029/1998JB900014.

Bosch, M., M. Zamora, and W. Utama (2002), Lithology discrimination from physical rock properties, *Geophysics*, *67*, 573–581, doi:10.1190/1.1468618.

Caers, J., T. Hoffman, S. Strebelle and X.-H. Wen (2006), Probabilistic integration of geologic scenarios, seismic, and production data—a West Africa turbidite reservoir case study, *Leading Edge*, *25*, 240–244.

Calvert, R. (2005), 4D technology: Where are we, and where are we going?, *Geophys. Prospect.*, *53*, 161–171, doi:10.1111/j.1365-2478.2004.00469.x.

Cardiff, M., and P. K. Kitanidis (2009), Bayesian inversion for facies detection: An extensible level set framework, *Water Resour. Res.*, *45*, W10416, doi:10.1029/2008WR007675.

Cassiani, G., and A. Binley (2005), Modeling unsaturated flow in a layered formation under quasi-steady state conditions using geophysical data constraints, *Adv. Water Resour.*, *28*, 467–477, doi:10.1016/j.advwatres.2004.12.007.

Chappell, N. A., and J. W. Lancaster (2007), Comparison of methodological uncertainty within permeability measurements, *Hydrol. Process.*, *21*(18), 2504–2514, doi:10.1002/hyp.6416.

Chen, J., S. Hubbard, J. Peterson, K. Williams, M. Fienen, P. Jardine, and D. Watson (2006), Development of a joint hydrogeophysical inversion approach and application to a contaminated fractured aquifer, *Water Resour. Res.*, *42*, W06425, doi:10.1029/2005WR004694.

Cirpka, O. A., and P. K. Kitanidis (2000), Sensitivity of temporal moments calculated by the adjoint-state method and joint inversing of head and tracer data, *Adv. Water Resour.*, *24*, 89–103, doi:10.1016/S0309-1708(00)00007-5.

Comas, X., L. Slater, and A. Reeve (2005), Geophysical and hydrological evaluation of two bog complexes in a northern peatland: Implications for the distribution of biogenic gasses at the basin scale, *Global Biogeochem. Cycles*, *19*, GB4023, doi:10.1029/2005GB002582.

Commer, M., and G. A. Newman (2008), New advances in three-dimensional controlled-source electromagnetic inversion, *Geophys. J. Int.*, *172*, 513–535, doi:10.1111/j.1365-246X.2007.03663.x.

Cumani, A. (1991), Edge-detection in multispectral images, *Cvgip-Graphical Models Image Process.*, *53*(1), 40–51, doi:10.1016/1049-9652(91)90018-F.

del Río, J. A., and S. Whitaker (2001), Electrohydrodynamics in porous media, *Transp. Porous Media*, *44*(2), 385–405, doi:10.1023/A:1010762226382.

Dennis, J. E., and R. B. Schnabel (1996), *Numerical Methods for Unconstrained Optimization and Nonlinear Equations*, SIAM, Philadelphia, Pa.

DeVolder, B., J. Glimm, J. W. Grove, Y. Kang, Y. Lee, K. Pao, D. H. Sharp, and K. Ye (2002), Uncertainty quantification for multiscale simulations, *J. Fluids Eng.*, *124*, 29–41, doi:10.1115/1.1445139.

Ditmar, P. (2002), Finding the shape of a local heterogeneity by means of a structural inversion with constraints, *Geophys. Prospect.*, *50*(2), 209–223, doi:10.1046/j.1365-2478.2002.00308.x.

Droske, M., and M. Rumpf (2004), A variational approach to nonrigid morphological image registration, *SIAM J. Appl. Math.*, *64*(2), 668–687, doi:10.1137/S0036139902419528.

Dullin, C., M. Zientkowska, J. Napp, J. Missbach-Guentner, H. W. Krell, F. Muller, E. Grabbe, L. F. Tietze, and F. Alves (2009), Semiautomatic landmark-based two-dimensional-three-dimensional image fusion in living mice: Correlation of near-infrared fluorescence imaging of Cy5.5-labeled antibodies with flat-panel volume computed tomography, *Mol. Imaging*, *8*(1), 2–14.

Fregoso, E. (2010), 3-D cross-gradient joint inversion of multiple geophysical data, Ph.D. thesis, 243 pp., CICESE, Ensenada, Mex.

Fregoso, E., and L. A. Gallardo (2009), Cross-gradients joint 3-D inversion with applications to gravity and magnetic data, *Geophysics*, *74*, L31–L42, doi:10.1190/1.3119263.

Furtney, J. K., and A. W. Woods (2006), Limitations in qualitative and quantitative analysis of time-lapse data due to fluid flow uncertainties, *J. Geophys. Eng.*, *3*, 194–205, doi:10.1088/1742-2132/3/2/010.

Gallardo, L. A. (2007a), Multiple cross-gradient joint inversion for geospectral imaging, *Geophys. Res. Lett.*, *34*, L19301, doi:10.1029/2007GL030409.

Gallardo, L. A. (2007b), Generalised joint inversion of multiple subsurface data under a common structural framework, paper presented at 69th EAGE Conference and Exhibition, London, 11–14 June.

Gallardo, L. A., and M. A. Meju (2003), Characterization of heterogeneous near-surface materials by joint 2-D inversion of dc resistivity and seismic data, *Geophys. Res. Lett.*, *30*(13), 1658, doi:10.1029/2003GL017370.

Gallardo, L. A., and M. A. Meju (2004), Joint two-dimensional DC resistivity and seismic travel time inversion with cross-gradients constraints, *J. Geophys. Res.*, *109*, B03311, doi:10.1029/2003JB002716.

Gallardo, L. A., and M. A. Meju (2007), Joint two-dimensional cross-gradient imaging of magnetotelluric and seismic traveltime data for structural and lithological classification, *Geophys. J. Int.*, *169*, 1261–1272, doi:10.1111/j.1365-246X.2007.03366.x.

Gallardo, L. A., M. A. Meju, and M. A. Flores-Perez (2005), A quadratic programming approach for joint image reconstruction: Mathematical and geophysical examples, *Inverse Probl.*, *21*, 435–452, doi:10.1088/0266-5611/21/2/002.

Gallardo, L. A., S. Fontes, M. A. Meju, P. de Lugao, and M. P. Buonora (2010), Joint cross-gradient inversion of offshore seismic reflection, MT, gravity and magnetic profiles over a petroliferous prospect in Santos basin, Brazil, paper presented at 20th Workshop on Electromagnetic Induction in the Earth, IAGA, Giza, Egypt, 18–24 Sept.

Gedney, N., P. M. Cox, and C. Huntingford (2004), Climate feedback from wetland methane emissions, *Geophys. Res. Lett.*, *31*, L20503, doi:10.1029/2004GL020919.

Gundlich, B., K.-R. Koch, and J. Kusche (2003), Gibbs sampler for computing and propagating large covariance matrices, *J. Geod.*, *77*, 514–528, doi:10.1007/s00190-003-0350-5.

Günther, T., and L. Bentley (2006), A new joint inversion algorithm applied to the interpretation of dc resistivity and refraction data, in *Proceedings of XVI International Conference on Computational Methods in Water Resources*, edited by P. J. Binning et al., 8 pp., Tech. Univ. of Den., Copenhagen.

Günther, T., C. Rucker, and K. Spitzer (2006), Three-dimensional modelling and inversion of dc resistivity data incorporating topography–II. Inversion, *Geophys. J. Int.*, *166*, 506–517, doi:10.1111/j.1365-246X.2006.03011.x.

Haber, E., and J. Modersitzki (2007), Intensity gradient based registration and fusion of multi-modal images, *Methods Inf. Med.*, *46*(3), 292–299.

Haber, E., and D. Oldenburg (1997), Joint inversion: A structural approach, *Inverse Probl.*, *13*, 63–77, doi:10.1088/0266-5611/13/1/006.

Handels, H., A. Horsch, and H. P. Meinzer (2007), Advances in medical image computing, *Methods Inf. Med.*, *46*(3), 251–253.

Hatchell, P., and S. Bourne (2005), Rocks under strain: Strain-induced time-lapse time shifts are observed for depleting reservoirs, *Leading Edge*, *24*, 1222–1225, doi:10.1190/1.2149624.

Hertrich, M., and U. Yaramanci (2002), Joint inversion of Surface Nuclear Magnetic Resonance and Vertical Electrical Sounding, *J. Appl. Geophys.*, *50*, 179–191, doi:10.1016/S0926-9851(02)00138-6.

Hole, J.A., C.A. Zelt and R.G. Pratt (2005), Advances in controlled-source seismic imaging, *Eos Trans. AGU*, *86*(18), 177.

Hu, W., A. Abubakar, and T. M. Habashy (2007), Integrated imaging and inversion of multi-physics data for exploration geophysics applications, in *2nd IEEE International Workshop on Computational Advances in Multi-sensor Adaptive Processing*, pp.169–172, IEEE Press, New York, doi:10.1109/CAMSAP.2007.4497992.

Hu, W. Y., A. Abubakar, and T. M. Habashy (2009), Joint electromagnetic and seismic inversion using structural constraints, *Geophysics*, *74*, R99–R109, doi:10.1190/1.3246586.

Hubbard, S. S., J. Chen, Y. Facng, K. Williams, S. Mukhopadhyay, E. Sonnenthal, K. McFarlane, N. Linde, and T. Scheibe (2006), Improved parameterization of hydrological models and reduction of geophysical monitoring data ambiguity through joint use of geophysical and numerical modeling methods, paper presented at XVI International Conference on Computational Methods in Water Resources, Copenhagen, 18–22 June.

Infante, V., L. A. Gallardo, J. C. Montalvo-Arrieta, and I. Navarro de Leon (2010), Lithological classification assisted by the joint inversion of electrical and seismic data at a control site in northeast Mexico, *J. Appl. Geophys.*, *70*, 93–102, doi:10.1016/j.jappgeo.2009.11.003.

Jackson, D. D. (1972), Interpretation of inaccurate, insufficient and inconsistent data, *Geophys. J. R. Astron. Soc.*, *28*, 97–110.

Jegen, M. D., R. W. Hobbs, P. Tarits, and A. Chave (2009), Joint inversion of marine magnetotelluric and gravity data incorporating seismic constraints: Preliminary results of sub-basalt imaging off the Faroe Shelf, *Earth Planet. Sci. Lett.*, *282*, 47–55, doi:10.1016/j.epsl.2009.02.018.

Kalscheuer, T., and L. B. Pedersen (2007), A non-linear truncated SVD variance and resolution analysis of two-dimensional magnetotelluric models, *Geophys. J. Int.*, *169*, 435–447, doi:10.1111/j.1365-246X.2006.03320.x.

Kalscheuer, T., M. A. G. Juanatey, N. Meqbel, and L. B. Pedersen (2010), Non-linear model error and resolution properties from two-dimensional single and joint inversions of direct current resistivity and radiomagnetotelluric data, *Geophys. J. Int.*, *182*, 1174–1188, doi:10.1111/j.1365-246X.2010.04686.x.

Kemna, A., A. Binley, and L. Slater (2004), Crosshole IP imaging for engineering and environmental applications, *Geophysics*, *69*, 97–107, doi:10.1190/1.1649379.

Kravaris, C., and J. H. Seinfeld (1985), Identification of parameters in distributed parameter systems by regularization, *SIAM J. Control Optim.*, *23*, 217–241, doi:10.1137/0323017.

Landrø, M. (2002), Uncertainties in quantitative time-lapse seismic analysis, *Geophys. Prospect.*, *50*(5), 527–538, doi:10.1046/j.1365-2478.2002.00330.x.

Lees, J., and J. VanDecar (1991), Seismic tomography constrained by bouguer gravity anomalies: Applications in western Washington, *Pure Appl. Geophys.*, *135*, 31–52, doi:10.1007/BF00877007.

Lelièvre, P. G. (2009), Integrating geologic and geophysical data through advanced constrained inversions, Ph.D. thesis, Univ. of B. C., Vancouver.

Lelièvre, P. G., and D. W. Oldenburg (2009), A comprehensive study of including structural orientation information in geophysical inversions, *Geophys. J. Int.*, *178*, 623–637, doi:10.1111/j.1365-246X.2009.04188.x.

Linde, N., A. Binley, A. Tryggvason, L. B. Pedersen, and A. Revil (2006), Improved hydrogeophysical characterization using joint inversion of cross-hole electrical resistance and ground penetrating radar traveltime data, *Water Resour. Res.*, *42*, W12404, doi:10.1029/2006WR005131.

Linde, N., A. Tryggvason, J. E. Peterson, and S. S. Hubbard (2008), Joint inversion of crosshole radar and seismic traveltimes acquired at the South Oyster Bacterial Transport Site, *Geophysics*, *73*, G29–G37, doi:10.1190/1.2937467.

Lines, L., A. Schultz, and S. Treitel (1988), Cooperative inversion of geophysical data, *Geophysics*, *53*, 8–20, doi:10.1190/1.1442403.

Looms, M. C., A. Binley, K. H. Jensen, L. Nielsen, and T. M. Hansen (2008), Identifying unsaturated hydraulic parameters using an integrated data fusion approach on cross-borehole geophysical data, *Vadose Zone J.*, *7*, 238–248, doi:10.2136/vzj2007.0087.

Lumley, D. (2001), Time-lapse seismic reservoir monitoring, *Geophysics*, *66*, 50–53, doi:10.1190/1.1444921.

Meju, M. A. (1994), Biased estimation: A simple framework for parameter estimation and uncertainty analysis with prior data, *Geophys. J. Int.*, *119*, 521–528, doi:10.1111/j.1365-246X.1994.tb00139.x.

Meju, M. A. (2005), Non-invasive characterisation of fractured crystalline rocks using a combined multicomponent transient electromagnetic, resistivity and seismic approach, in *Petrophysical Properties of Crystalline Rocks*, vol. 240, edited by P. K. Harvey, pp. 195–206, Geol. Soc. of London, London.

Meju, M. A. (2009), Regularized extremal bounds analysis (REBA): An approach to quantifying uncertainty in nonlinear geophysical inverse problems, *Geophys. Res. Lett.*, *36*, L03304, doi:10.1029/2008GL036407.

Meyer, M., J.-P. Hermund, M. Asch, and J.-C. Le Gac (2006), An analytic multiple frequency adjoint-based inversion algorithm for parabolic-type approximations in ocean acoustics, *Inverse Probl. Sci. Eng.*, *14*, 245–265, doi:10.1080/17415970500408023.

Minkoff, S. E., C. M. Stone, S. Bryant, and M. Peszynska (2004), Coupled geomechanics and flow simulation for time-lapse seismic modeling, *Geophysics*, *69*, 200–211, doi:10.1190/1.1649388.

Musil, M., H. R. Maurer, and A. G. Green (2003), Discrete tomography and joint inversion for loosely connected or unconnected physical properties: Application to crosshole seismic and georadar data sets, *Geophys. J. Int.*, *153*, 389–402, doi:10.1046/j.1365-246X.2003.01887.x.

Nocedal, J., and S. J. Wright (1999), *Numerical Optimization*, Springer, New York, doi:10.1007/b98874.

Norton, S. J. (1999), Iterative inverse scattering algorithms: Methods of computing Frechet derivatives, *J. Acoust. Soc. Am.*, *106*(5), 2653–2660, doi:10.1121/1.428095.

Oldenburg, D. W., Y. Li, and R. G. Ellis (1997), Inversion of geophysical data over a copper gold porphyry deposit–a case history for Mt. Milligan, *Geophysics*, *62*, 1419, doi:10.1190/1.1444246.

Orange, A., K. Key, and S. Constable (2009), The feasibility of reservoir monitoring using time-lapse marine CSEM, *Geophysics*, *74*, F21–F29, doi:10.1190/1.3059600.

Paasche, H., and J. Tronicke (2007), Cooperative inversion of 2D geophysical data sets: A zonal approach based on fuzzy *c*-means cluster analysis, *Geophysics*, *72*, A35–A39, doi:10.1190/1.2670341.

Paasche, H., J. Tronicke, K. Holliger, A. G. Green, and H. Maurer (2006), Integration of diverse physical-property models: Subsurface zonation and petrophysical parameter estimation based on fuzzy *c*-means cluster analyses, *Geophysics*, *71*, H33–H44, doi:10.1190/1.2192927.

Parker, J. R. (1997), *Algorithms for Image Processing and Computer Vision*, 1st ed., 417 pp., John Wiley, New York.

Pride, S. (1994), Governing equations for the coupled electromagnetics and acoustics of porous media, *Phys. Rev. B*, *50*(21), 15,678–15,696, doi:10.1103/PhysRevB.50.15678.

Reagan, M. T., H. N. Najm, R. G. Ghanem, and O. M. Knio (2003), Uncertainty quantification in reacting-flow simulations through non-intrusive spectral projection, *Combust. Flame*, *132*, 545–555, doi:10.1016/S0010-2180(02)00503-5.

Rickett, J., L. Duranti, T. Hudson, and B. Regel (2007), 4D time strain and the seismic signature of geomechanical compaction at Genesis, *Lead. Edge*, *26*, 644–647, doi:10.1190/1.2737103.

Rodi, W., and R. L. Mackie (2001), Nonlinear conjugate gradients algorithm for 2-D magnetotelluric inversions, *Geophysics*, *66*, 174–187, doi:10.1190/1.1444893.

Roecker, S., C. Thurber, and D. McPhee (2004), Joint inversion of gravity and arrival time data from Parkfield: New constraints on structure and hypocenter locations near the SAFOD drill site, *Geophys. Res. Lett.*, *31*, L12S04, doi:10.1029/2003GL019396.

Sasaki, Y. (1989), Two-dimensional joint inversion of magnetotelluric and dipole-dipole resistivity data, *Geophysics*, *54*, 254–262, doi:10.1190/1.1442649.

Sasaki, Y. (2004), Three-dimensional inversion of static-shifted magnetotelluric data, *Earth Planets Space*, *56*, 239–248.

Sasaki, Y., and M. A. Meju (2006a), Three-dimensional joint inversion for magnetotelluric resistivity and static shift distributions in complex media, *J. Geophys. Res.*, *111*, B05101, doi:10.1029/2005JB004009.

Sasaki, Y., and M. A. Meju (2006b), A multidimensional horizontal-loop controlled-source electromagnetic inversion method and its use to characterize aquiferous fractured crystalline rocks, *Geophys. J. Int.*, *166*, 59–66, doi:10.1111/j.1365-246X.2006.02957.x.

Shin, C., K. Yoon, K. J. Marfut, K. Park, D. Yang, H. Y. Lim, S. Chung, and S. Shin (2001), Efficient calculation of a partial-derivative wavefield using reciprocity for seismic imaging and inversion, *Geophysics*, *66*, 1856–1863, doi:10.1190/1.1487129.

Siripunvaraporn, W., G. Egbert, Y. Lenbury, and M. Uyeshima (2005), Three-dimensional magnetotelluric inversion: Data-space method, *Phys. Earth Planet. Inter.*, *150*, 3–14, doi:10.1016/j.pepi.2004.08.023.

Snieder, R. (2004), Uncertainty estimation in inverse problems: An uncertain proposition, *Eos Trans. AGU*, *85*(47), Fall Meet. Suppl., Abstract NG33B-01.

Toivanen, P. J., J. Ansamaki, J. P. S. Parkkinen, and J. Mielikainen (2003), Edge detection in multispectral images using the self-organizing map, *Pattern Recognit. Lett.*, *24*(16), 2987–2994, doi:10.1016/S0167-8655(03)00159-4.

Tryggvason, A., and N. Linde (2006), Local earthquake (LE) tomography with joint inversion for P- and S-wave velocities using structural constraints, *Geophys. Res. Lett.*, *33*, L07303, doi:10.1029/2005GL025485.

Tsuneyama, F., and G. Mavko (2007), Quantitative detection of fluid distribution using time-lapse seismic, *Geophys. Prospect.*, *55*(2), 169–184, doi:10.1111/j.1365-2478.2007.00605.x.

Vasco, D. W. (2007), Invariance, groups, and non-uniqueness: The discrete case, *Geophys. J. Int.*, *168*, 473–490, doi:10.1111/j.1365-246X.2006.03161.x.

Vozoff, K., and D. L. B. Jupp (1975), Joint inversion of geophysical data, *Geophys. J. R. Astron. Soc.*, *42*, 977–991, doi:10.1111/j.1365-246X.1975.tb06462.x.

Zhang, J., and F. D. Morgan (1997), Joint seismic and electrical tomography, paper presented at Symposium on Applications of Geophysics to Engineering and Environmental Problems, EEGS, Keystone, Colo.

L. A. Gallardo, School of Earth and Environment, University of Western Australia, Crawley, WA 6009, Australia. (luis.gallardo@uwa.edu.au)

M. A. Meju, Petronas Research, 43000 Kajang, Malaysia. (maxwell_meju@petronas.com.my)